nature plants

ARTICLES

https://doi.org/10.1038/s41477-020-0681-8

DHH1/DDX6-like RNA helicases maintain ephemeral half-lives of stress-response mRNAs

Thanin Chantarachot[1], Reed S. Sorenson[2], Maureen Hummel[1], Haiyan Ke[1], Alek T. Kettenburg[1], Daniel Chen[1], Karen Aiyetiwa[1], Katayoon Dehesh[1], Thomas Eulgem[1], Leslie E. Sieburth[2] and Julia Bailey-Serres[1]✉

Gene transcription is counterbalanced by messenger RNA decay processes that regulate transcript quality and quantity. We show here that the evolutionarily conserved DHH1/DDX6-like RNA hellicases of *Arabidopsis thaliana* control the ephemerality of a subset of cellular mRNAs. These RNA helicases co-localize with key markers of processing bodies and stress granules and contribute to their subcellular dynamics. They function to limit the precocious accumulation and ribosome association of stress-responsive mRNAs involved in auto-immunity and growth inhibition under non-stress conditions. Given the conservation of this RNA helicase subfamily, they may control basal levels of conditionally regulated mRNAs in diverse eukaryotes, accelerating responses without penalty.

The dynamic regulation of messenger RNA translation, decay and sequestration is essential for growth, development and responses to internal and external stimuli. These processes involve interconnected mRNA–ribonucleoprotein (mRNP) complexes, including poly(ribo)somes, processing bodies (PBs) and stress granules (SGs)[1]. Depending on the biological context, mRNAs targeted to PBs can be degraded or stabilized[2,3] whereas those sequestered in SGs are generally stabilized[4,5].

In eukaryotes, the bulk of cytoplasmic mRNAs are degraded by general decay pathways initiated by deadenylation of the poly(A) tail. This can be followed by 5′-to-3′ decay that requires mRNA decapping or 3′-to-5′ decay by the RNA exosome or the exoribonuclease SUPPRESSOR OF VARICOSE (SOV/DIS3L2), which is non-functional in *Arabidopsis* Columbia-0 (Col-0) but controls mRNA abundance and homeostasis when replaced by SOV of Landsberg *erecta*[6,7]. The decapping pathway requires the decapping enzyme DECAPPING 2 (DCP2) and core decapping factors DCP1 and VARICOSE (VCS/EDC4/HEDLS), and is facilitated by conserved decapping activators such as DCP5, PROTEIN ASSOCIATED WITH TOPOISOMERASE 1 (PAT1), the LSM1-7 complex and DHH1/DDX6 (CGH-1/Me31B/Xp54)[8]. Decapped mRNAs can be hydrolysed by the 5′-to-3′ exoribonuclease XRN1/4 (ref. [9]). These 5′ and 3′ pathways have substrate specificity, yet they are not mutually exclusive.

Spatiotemporal regulation of mRNA decay is critical for the cellular transcriptome adjustment in response to both developmental and environmental cues in plants[1]. Dysfunction in decapping due to loss of function of non-redundant components results in post-embryonic lethality (DCP1, DCP2, VCS and DCP5) or severe growth alterations (LSM1 and PAT1)[10–14]. The cause of the developmental defects in certain decapping mutants is associated with disruption of mRNA quality control and small interfering RNA (siRNA) production[15]. However, there is limited knowledge about the role of the decay machinery in the spatial and temporal turnover of specific mRNAs, and the connections between turnover and mRNA translation and mobilization to PBs and SGs. Mutations in the mRNA decay machinery have been identified in genetic screens for altered sensitivity to biotic and abiotic stresses[14,16–19], yet there is poor understanding of the importance of mRNA decay in restricting accumulation of mRNAs that provide stress resilience but constrain growth.

The DHH1/DDX6 family of DEAD-box RNA helicases is conserved across eukaryotes[20]. These proteins function at the nexus between mRNA translation, storage and decay, mediating translational repression and initiating mRNA degradation[21–24]. For example, yeast DHH1 was shown to activate mRNA decapping[25] and promote translational repression[26], and also to associate with ribosomes to sense the codon-dependent rate of translational elongation and trigger decay[27]. However, the transcript-specific role of these helicases is generally understudied. Here we identify the *Arabidopsis* DHH1/DDX6-like proteins RNA HELICASE 6 (RH6), RH8 and RH12 as functionally redundant mRNA decay factors required for normal growth and development. Severe deficiency of *RH6*, *RH8* and *RH12* function affects PB and SG dynamics and shifts the transcriptome and translatome homeostasis so that defence- and other stress-responsive mRNAs accumulate despite growth under standard conditions, with simultaneous repression of mRNAs required for general growth. RNA decay analysis determined that these RHs facilitate the turnover of specific short-lived decapping substrates, enriched for stress and defence responses. Stabilization of these ephemeral mRNAs in the *rh6812* mutant confers auto-immunity. We propose that RH-mediated decay of stress-responsive mRNAs under non-stress conditions is required for maintenance of the growth/defence balance in plants.

Results

***Arabidopsis* RH6, RH8 and RH12 are essential DHH1/DDX6-like proteins.** The Viridiplantae encode DHH1/DDX6-like proteins with a dual RecA helicase core, including *Arabidopsis thaliana* RH6 (At2g45810), RH8 (At4g00660) and RH12 (At3g61240) (Fig. 1a and Extended Data Fig. 1). These three RHs share 79–86% protein sequence identity, and their transcripts are generally co-expressed

[1]Center for Plant Cell Biology, Department of Botany and Plant Sciences, University of California, Riverside, Riverside, CA, USA. [2]School of Biological Sciences, University of Utah, Salt Lake City, UT, USA. ✉e-mail: serres@ucr.edu

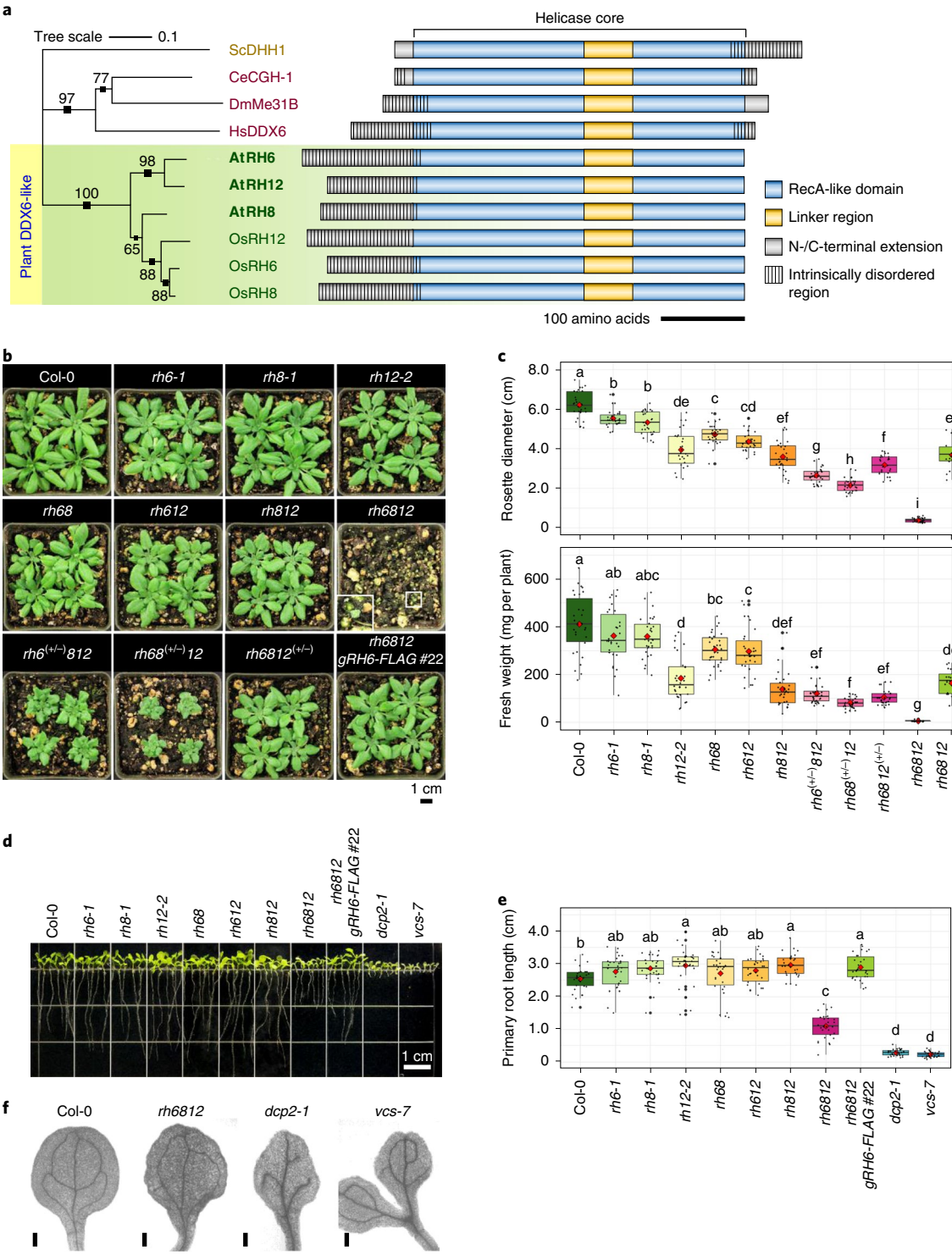

Fig. 1 | *Arabidopsis RH6, RH8 and RH12* overlap in their contribution to growth and development. a, Phylogenetic relationship and schematic diagram of DHH1/DDX6-like proteins from the yeast *Saccharomyces cerevisiae* (ScDHH1), roundworm (CeCGH-1), fruit fly (DmMe31B), human (HsDDX6), *Arabidopsis* (AtRH6, AtRH8 and AtRH12) and rice (OsRH6, OsRH8 and OsRH12). The tree is to scale, with branch lengths measured as the number of substitutions per site. Numbers on branches indicate bootstrap values. Bold text highlights the DHH1/DDX6-like proteins. **b**, Rosette growth phenotype of 39-day-old plants of Col-0 wild type in comparison to the single (*rh6-1*, *rh8-1* and *rh12-2*), double (*rh68*, *rh612* and *rh812*), double homozygous hemizygous (*rh6*$^{(+/-)}$*812*, *rh68*$^{(+/-)}$*12* and *rh6812* $^{(+/-)}$) and triple (*rh6812*; inset) mutant combinations, and a transgenic line homozygous for the *rh6812* triple-mutant alleles with an introduced genomic *RH6* wild-type allele C-terminally tagged with the FLAG epitope (*rh6812 gRH6-FLAG* #22). Seeds were grown directly on soil; representative plants were selected. **c**, Rosette diameter ($n = 28$) and fresh weight ($n = 30$) of 39-day-old plants in **b**. **d**, 7-day-old seedlings. **e**, Primary root length ($n = 15$) of seedlings in **d**. **f**, Representative images of the cotyledon vasculature of 7-day-old seedlings of Col-0 wild-type, *rh6812*, *dcp2-1* and *vcs-7* mutants ($n = 30$ per genotype). Scale bars, 0.3 mm. Boxplot boundaries in **c**,**e** represent the first and third quartiles; a horizontal line divides the interquartile range, median; red diamonds, mean. Means significantly different between genotypes are indicated by different letters ($P < 0.05$, analysis of variance (ANOVA) with Tukey's honest significant difference (HSD) test). See Source Data for *P* values.

(Supplementary Fig. 1). Single-gene mutants *rh6-1*, *rh8-1* and *rh12-2*, which produce little to no detectable protein, have slightly reduced rosette size and fresh weight relative to the wild type (*SOV*-deficient Col-0 background) (Fig. 1b,c and Extended Data Fig. 2). To test whether they are functionally redundant, double *rh68* (that is, *rh6-1 rh8-1*), *rh612* and *rh812* mutants, and a triple *rh6812* mutant, were generated and evaluated for RH protein level and phenotype. We found that rosette growth is generally proportional to functional *RH* gene copies, with the triple mutant *rh6812* displaying extremely diminished rosette diameter and fresh weight (Fig. 1b,c and Supplementary Fig. 2). Independent hypomorphic *amiRH6 rh812* lines with strong partial suppression of *RH6* transcripts displayed less evident seedling alterations but had significantly reduced rosette growth (Extended Data Fig. 3a–h). Growth and reproduction of *rh6812* were rescued by the introduction of a 3.3-kb genomic fragment of *RH6* with a C-terminal FLAG epitope tag (*gRH6-FLAG*), because the *rh6812 gRH6-FLAG* plants had rosette growth similar to the equivalent genotype *rh812* (Fig. 1b,c and Extended Data Fig. 4a–e).

Arabidopsis decapping mutants display seedling phenotypes, including shortened primary roots[10,12,13]. The *rh* single and double mutants, as well as *amiRH6 rh812* lines and *rh6812 gRH6-FLAG* homozygotes, had seedling roots of length similar or longer than that of Col-0, whereas *rh6812* roots were significantly shorter (Fig. 1d,e and Extended Data Fig. 4g,h). However, *rh6812* roots were significantly longer than those of the decapping mutants *dcp2-1* and *vcs-7* (Fig. 1d,e). These three genotypes shared small cotyledons with disorganized veins (Fig. 1f). We conclude that *RH6*, *RH8* and *RH12* have highly overlapping and additive functions in regulating multiple aspects of growth and development.

Severe growth defects exhibited by mRNA decay mutants can be partly due to the accumulation of siRNA produced from aberrant RNAs[15,28]. Developmental defects of *dcp2-1* and *vcs-6* are partially rescued by mutation of *RNA-DEPENDENT RNA POLYMERASE 6* (*RDR6*)[15]. The *rh6812* growth phenotype is not primarily due to RDR6-mediated gene silencing, as neither the quadruple *rh6812 rdr6*$^{sgs2\text{-}1}$ nor the *rh6812 sgs3-1* (*suppressor of gene silencing 3-1*) genotype was rescued (Extended Data Fig. 5a,b).

RH6, RH8 and RH12 are nucleocytoplasmic and associate with PBs and SGs. The subcellular localizations of the three RHs were determined with transgenic lines that individually express genomic *RH6*, *RH8* or *RH12* translationally fused with a C-terminal red fluorescent protein (*gRH6-RFP*, *gRH8-RFP* or *gRH12-RFP*). All three RH-RFPs were nucleocytoplasmic in the root meristem region of seedlings grown under standard conditions (Fig. 2a,b and Supplementary Fig. 3a–f). The RH N-terminal region contains glutamine- and proline-rich sequences predicted to be intrinsically disordered (Fig. 1a), a property that facilitates the formation of macromolecular condensates through liquid–liquid phase separation[29]. This was evaluated in the cortex cells of the root meristematic zone. Seedlings were bathed in water, placed under a coverslip and imaged within 2 min and again after 30 min. RH6-RFP was initially cytoplasmically dispersed and then present in large foci (Fig. 2c). These foci represent mRNP complexes, because the pretreatment of seedlings with cycloheximide inhibited the formation of RH6 foci altogether. Translation termination-dependent foci were similarly observed for RH8 and RH12 (Supplementary Fig. 3g,h). We conclude that these RHs form mRNP assemblies with mRNAs released from polysomes.

Next, we considered whether RH6, RH8 and RH12 are targeted to the same mRNPs. Root cortical cells co-expressing *gRH6-RFP* and *gRH8-GFP* co-localized both proteins in nearly all detectable cytoplasmic foci (Fig. 2d). The pairwise evaluation of all three RHs confirmed that all co-localize in foci (Supplementary Fig. 4a–c). We asked whether RH-containing foci are PBs or SGs. By the use of two GFP-tagged PB (DCP2 and VCS) markers, we resolved DCP2 assemblies after 2 min, which enlarged after 30 min and often co-localized with RH6 (Fig. 2d and Supplementary Fig. 5a). The lack of complete overlap of the RH6 and DCP2 foci suggests heterogeneity in mRNP formation, functional subdomains and dynamics. Similar co-localization dynamics were observed for RH8 and RH12 with DCP2 (Supplementary Fig. 5b,c) and VCS-GFP expressed under its native promoter (Fig. 2d and Supplementary Fig. 6a–c).

The incomplete association of RHs with DCP2 and VCS led us to test whether RHs overlap with the SG marker OLIGOURIDYLATE-BINDING PROTEIN 1 C (UBP1C), a mammalian TIA-1/TIAR orthologue known to be dynamically and reversibly induced within 25 min by coverslip-induced hypoxia[4]. We confirmed overlap of UBP1C and RH foci within 2 min, which increased after 30 min, in both foci size and number, in the root meristem of seedlings co-expressing the *gRH-RFPs* and *pro35S:UBP1C-GFP* (Fig. 2d and Supplementary Fig. 7a–c). Borders of the complexes were enriched for one or the other protein. We conclude that assemblies containing the three RHs dynamically associate with both PBs and SGs to form hybrid and heterogenous mRNP complexes.

RH6, RH8 and RH12 contribute to the assembly of PB and SG complexes. To determine whether RH function influences the formation of PB and SG assemblies, foci were examined in *rh6812* mutants expressing DCP2-GFP, VCS-GFP or UBP1C-GFP. In contrast to DCP2 and VCS assembly dynamics in the root meristem of Col-0, these markers were in significantly fewer foci at both 2 and 30 min in *rh6812* (Fig. 2e,f,h). The size of DCP2 foci increased in both Col-0 and *rh6812*, but VCS foci increased only in Col-0 (Fig. 2i). The deficiency in RHs also limited the temporal increase in number but not the size of UBP1C-containing SGs. These data provide further evidence of PB heterogeneity and indicate that RHs contribute to the formation of large PBs and SGs.

***RH6*, *RH8* and *RH12* are required for transcriptome and translatome homeostasis.** Because the *rh6812* genotype had dampened

Fig. 2 | RH6, RH8 and RH12 form cytoplasmic mRNPs contributing to PB and SG formation. a, RFP fluorescence in root tissues of 4-day-old *genomic(g) RH6-RFP* seedlings. Left, maximum projection of 12 *z*-planes evenly spread across 55 µm; right, overlay on bright field image. Scale bars, 100 µm. **b**, Root meristem of seedlings in **a** counterstained with 4′,6-diamidino-2-phenylindole (DAPI) for nuclear visualization. Lower panels, magnification of framed areas in upper panels. **c**, Subcellular localization of RH6-RFP in the root meristem of 4-day-old seedlings submerged in water under a coverslip for 2 min, and the same regions re-imaged after 30 min. Seedlings pretreated with 0.001% (v/v) dimethyl sulfoxide (DMSO) with or without cycloheximide (CHX) for 3 min by vacuum infiltration before imaging. Images in **a**–**c** are representative of individual genotypes from two independent experiments with similar results. **d**, Co-localization of RFP and green fluorescent protein (GFP) signals in the root meristem of 4-day-old seedlings co-expressing *gRH6-RFP* with *gRH8-GFP*, *proDCP2:DCP2-GFP*, *proVCS:VCS-GFP* or *pro35S:UBP1C-GFP*. Imaging as described for **c**. RFP signals, false-coloured magenta. Arrowheads denote examples of foci with co-localized RFP and GFP signals. **e**–**g**, GFP fluorescence of DCP2-GFP (**e**), VCS-GFP (**f**) and UBP1C-GFP (**g**) in the root meristem of Col-0 or *rh6812*. Developmental age-matched 4-day-old seedlings were imaged as in **c**. Images representative of $n \geq 6$ seedlings per genotype. Scale bars in **b**–**g**, 10 µm. **h**,**i**, Quantification of number (**h**) and size (**i**) of DCP2-GFP (Col-0, $n = 9$; *rh6812*, $n = 12$), VCS-GFP ($n = 10$) and UBP1C-GFP ($n = 8$) foci. Boxplot boundaries represent the first and third quartiles; a horizontal line divides the interquartile range, median. Means significantly different between genotypes are indicated by different letters (Kruskal–Wallis test followed by two-sided Wilcoxon test). See Source Data for *P* values.

PB and SG formation, we hypothesized that RHs might contribute to the regulation of transcript abundance and translation. We established the genotype *rh6812* expressing an epitope-tagged RIBOSOMAL PROTEIN L18 that enables translating ribosome affinity purification (TRAP)[30], to magnetically capture transcripts associated with ribosomes and thereby engaged in translation.

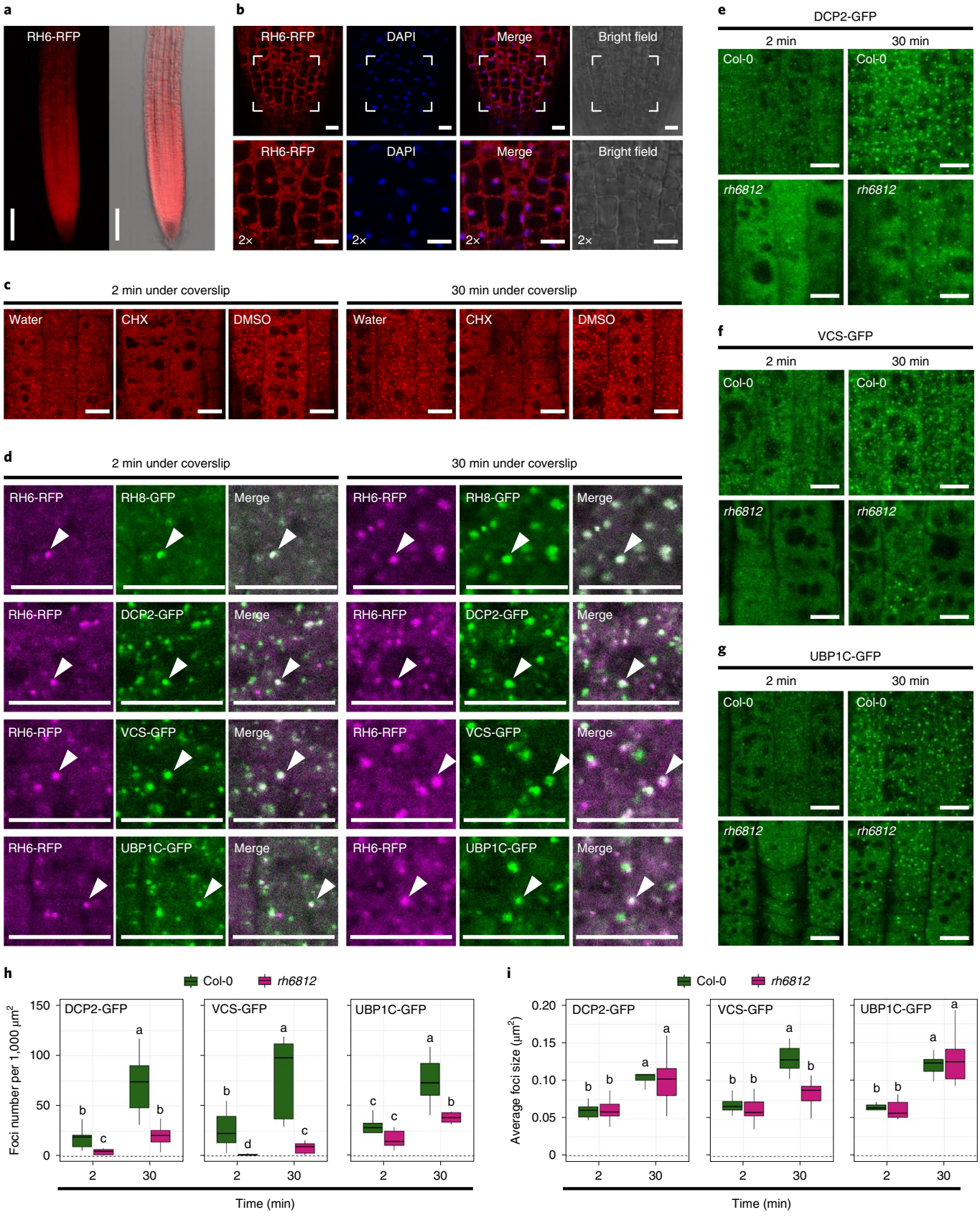

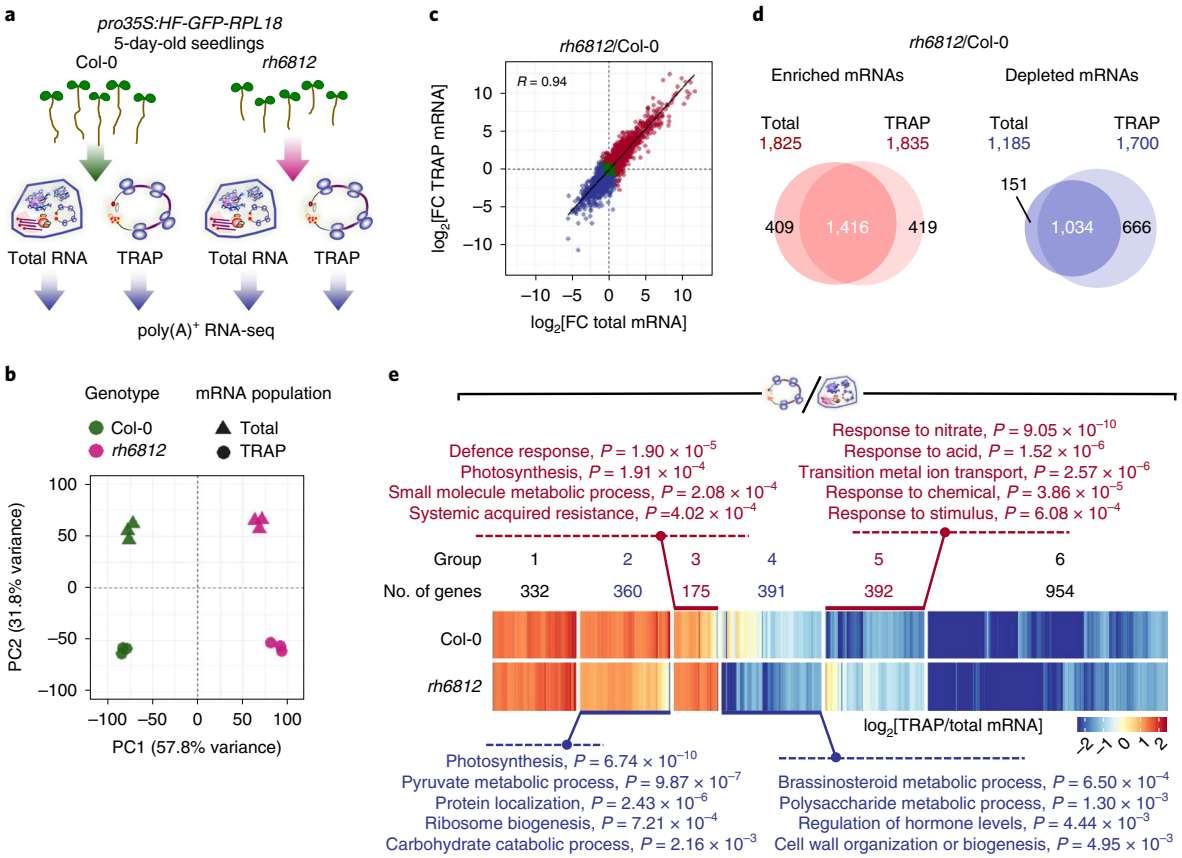

Fig. 3 | Attenuation of *RH6*, *RH8* and *RH12* function shifts the seedling steady-state transcriptome and translatome from a general growth to stress-responsive state. a, Schematic representation of experimental set-up for transcriptome and translatome analyses. Ribosome-associated RNAs were isolated from developmental age-matched 5-day-old seedlings of Col-0 and *rh6812*, both expressing His-FLAG-GFP-tagged RIBOSOMAL PROTEIN L18 (*pro35S:HF-GFP-RPL18*) using TRAP. PolyA$^+$ RNA (total) was isolated from the same tissue. **b**, Principal component (PC) analysis of edgeR-normalized read counts of total and TRAP mRNAs from Col-0 and *rh6812* ($n = 3$ biologically independent samples per genotype). **c**, Scatter plot comparison of $\log_2$[FC] between total and TRAP mRNAs in *rh6812* relative to Col-0 ($n = 14{,}391$ genes). *R* represents Pearson correlation coefficient of significantly enriched and depleted genes (red and blue dots, $|\log_2[FC]| \geq 1$, FDR < 0.01 in either RNA populations, $n = 4{,}089$). **d**, Overlap of genes significantly enriched or depleted in *rh6812* relative to Col-0 ($|\log_2[FC]| \geq 1$, FDR < 0.01). **e**, Heatmap comparing 2,604 genes with efficient or poor translation status in Col-0 or *rh6812* ($|\log_2[TRAP/total\ mRNA]| \geq 1$, FDR < 0.01). These were classified into six groups based on the patterns of their translational status between the two genotypes. Number of genes in each group is shown. For each group, representative enriched GO terms were determined by a hypergeometric test; Bonferroni-adjusted *P* values given.

This enabled comparison of *rh6812* and Col-0 seedling poly(A)$^+$ mRNA (total mRNA; transcriptome) and ribosome-associated poly(A)$^+$ mRNA (TRAP mRNA; translatome) (Fig. 3a). RNA-sequencing was performed on triplicate biological samples to an average depth of 19.4 million reads, revealing reproducible differences between the two genotypes and two mRNA populations (Fig. 3b, Extended Data Fig. 6a and Supplementary Table 1). Alterations in the transcriptome of the *rh6812* mutant were highly similar to alterations in its translatome (Pearson correlation = 0.94) (Fig. 3c), with 409 and 419 mRNAs uniquely enriched and 151 and 666 mRNAs uniquely depleted in the total and TRAP comparisons (*rh6812* relative to Col-0), respectively (Fig. 3d). The *rh6812* transcriptome and translatome were enriched in mRNAs with Gene Ontology (GO) functions associated with stress and innate immunity, and depleted of mRNAs associated with general growth and primary metabolism, including polysaccharide metabolic process, rhythmic process, multi-dimensional cell growth and regulation of hormone levels (Extended Data Fig. 6b and Supplementary Table 2).

Next, we investigated the impact of RH deficiency on translational status, the proportion of individual polyA$^+$ mRNAs associated with ribosomes. The global translation was similar in *rh6812* and Col-0 seedlings based on the quantitation of ribosomal subunits and polysome complexes by sucrose density gradient fractionation analyses (Supplementary Fig. 8). Nevertheless, the translation status of individual mRNAs varied in both Col-0 and *rh6812* seedlings (Extended Data Fig. 6c and Supplementary Table 1). Focusing on the 2,604 mRNAs with optimal and suboptimal translation status in at least one genotype ($|\log_2[FC]| \geq 1$ where FC is fold change, false discovery rate (FDR) < 0.01), we resolved groups with similar (groups 1 and 6) or distinct (groups 2–5) translational status in the two genotypes (Fig. 3e and Supplementary Table 3). mRNAs with higher translation status in Col-0 than in *rh6812* were associated with primary metabolism, protein localization and ribosome biogenesis in group 2, and brassinosteroid metabolic process, polysaccharide metabolic process and cell wall organization or biogenesis in group 4. Conversely, higher translational status was evident in *rh6812* for mRNAs associated with the defence response and systemic acquired resistance in group 3, and with responses to different stimuli in group 5 (Fig. 3e). This demonstrates that RHs contribute to transcriptome and translatome homeostasis under non-stress conditions by directly or indirectly promoting the ribosome association of mRNAs associated with growth and development, while

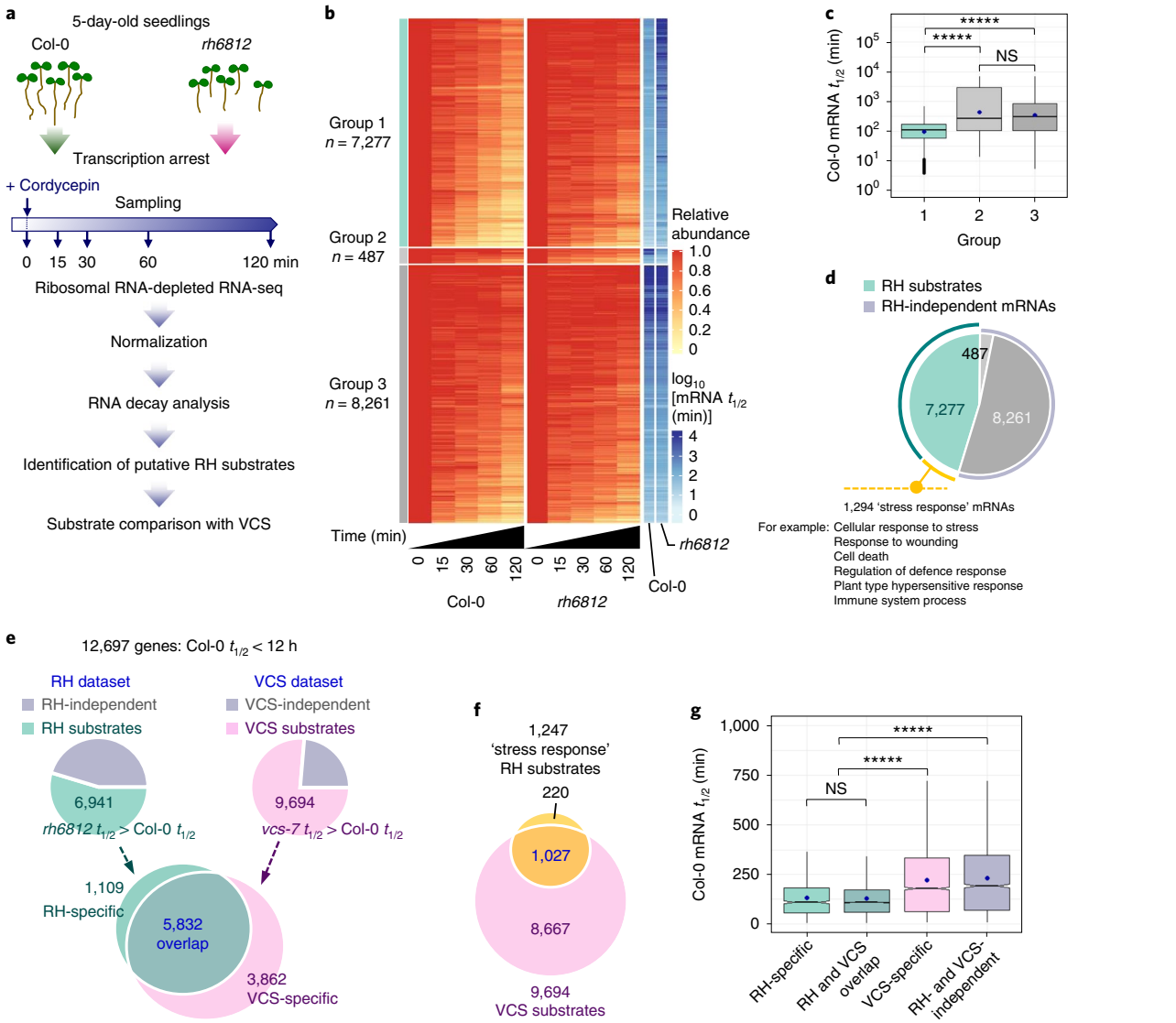

Fig. 4 | RHs facilitate decay of short-lived mRNAs. a, Experimental design for global RNA decay analysis. Seedlings were sampled at five time points after cordycepin treatment in biological triplicate. RNA-seq libraries were generated from total RNA following rRNA depletion. **b**, Heatmap of mRNA decay over 120 min and $t_{1/2}$ of 16,025 transcripts in Col-0 and *rh6812*. mRNA decay is presented as a change in mean relative mRNA abundance and hierarchically clustered into three groups. Group 1 mRNAs decreased decay rates in *rh6812* (putative RH substrates; $n = 7,277$; *rh6812* $t_{1/2}$ > Col-0 $t_{1/2}$); group 2 mRNAs increased decay rates in *rh6812* ($n = 487$; *rh6812* $t_{1/2}$ < Col-0 $t_{1/2}$); group 3 mRNAs were unaffected ($n = 8,261$; *rh6812* $t_{1/2} \simeq$ Col-0 $t_{1/2}$). **c**, Comparison of Col-0 mRNA $t_{1/2}$ between each group in **b**. *****$P < 2.2 \times 10^{-16}$; NS ($P = 0.086$), not significant (two-sided Wilcoxon test). **d**, Pie chart highlighting the proportion of RH substrates identified in **b** involved in stress or defence responses based on GO enrichment. **e**, Pie charts showing the proportion of putative substrates of RH (group 1) and VCS; Venn diagrams showing overlap between the populations. RH and VCS substrates are stabilized in *rh6812* and *vcs-7*, respectively. *vcs-7* mRNA decay data were modelled exactly as for RH, with comparison limited to genes with Col-0 mRNA $t_{1/2} < 12$ h. **f**, Venn diagram comparing overlap of RH substrates related to stress response with VCS-dependent decapping pathway substrates. **g**, Boxplots comparing the Col-0 $t_{1/2}$ of RH substrates and RH and VCS substrates classified in **e**. *****$P < 2.2 \times 10^{-16}$; NS ($P = 0.59$), not significant (two-sided Wilcoxon test). Boxplot boundaries in **c**,**g** represent the first and third quartiles; a horizontal line divides the interquartile range, median; blue circles, mean.

limiting that of mRNAs involved in the cellular response to stress and external stimuli.

RH6, RH8 and RH12 facilitate decay of select short-lived mRNAs. Co-localization of RHs with the decapping proteins DCP2 and VCS prompted an evaluation of their role in the decay of stress/stimuli-responsive and other mRNAs. This commenced with infiltration of *rh6812* and Col-0 seedlings with the transcription inhibitor cordycepin, sampling after 0, 15, 30, 60 and 120 min, and RNA-sequencing (RNA-seq) of ribosomal RNA-depleted total RNA (Fig. 4a). Triplicate biological samples were sequenced to an average depth of 22.7 million reads. After data normalization and exclusion of low-abundance mRNAs, transcript abundances were used to model decay rates for each gene and genotype[7].

We found that loss of RHs increased the stability of otherwise rapidly degraded transcripts, with the minimum and median mRNA half-life ($t_{1/2}$) increased from 3.8 and 160.9 min in Col-0 to 5.2 and 314.1 min in *rh6812*, respectively (Supplementary Fig. 9). This was also evident when the mRNAs were classified into three groups by the relative effect of RH deficiency on $t_{1/2}$ (Fig. 4b and

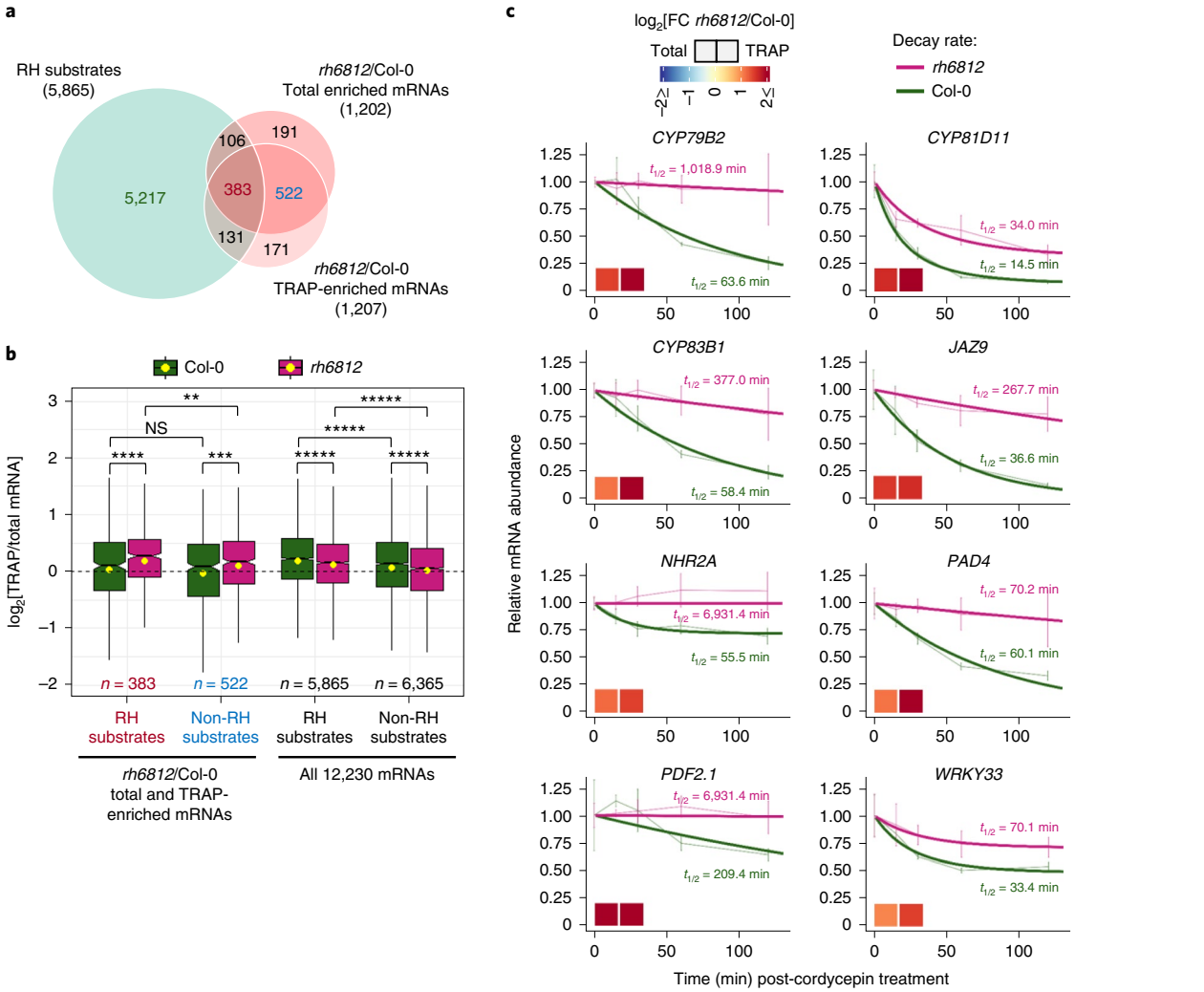

Fig. 5 | Stabilization of stress-response mRNAs in the *rh6812* genotype is associated with an increase in abundance and translational status. a, Venn diagram showing the overlap between RH decay substrates and steady-state total and TRAP mRNAs enriched in *rh6812* relative to Col-0 ($\log_2$ FC ≥ 1, FDR < 0.01) from a combined analysis of mRNA decay, transcriptome and translatome data comprising 12,230 genes. **b**, Boxplot comparing translational status ($\log_2$[TRAP/total mRNA]) of RH substrates and RH-independent mRNAs enriched in both total and TRAP fractions of *rh6812* relative to Col-0 ($n = 905$). *****$P < 2.2 \times 10^{-16}$, ****$P = 1.2 \times 10^{-13}$, ***$P = 3.4 \times 10^{-9}$, **$P = 0.011$; NS ($P = 0.2934$), no significant difference (two-sided Wilcoxon test). Boxplot boundaries represent the first and third quartiles; a horizontal line divides the interquartile range, median; yellow circles, mean. **c**, Decay profiles of representative stress- and defence-response mRNAs with an increase in total and TRAP mRNA abundance ($\log_2$[FC], indicated by coloured boxes) and translational status in *rh6812* relative to Col-0. mRNA decay profile of each genotype is presented as relative mRNA abundance after inhibition of transcription by cordycepin treatment (thin lines, mean ± s.e.m., $n = 3$ biologically independent samples per genotype) along with modelled value (thick lines). $t_{1/2}$ for each genotype is shown.

Supplementary Table 4). Group 1 ($n = 7,277$) mRNAs decayed more slowly in *rh6812* (*rh6812* $t_{1/2}$ > Col-0 $t_{1/2}$). These are termed RH substrates, because the presence of RHs in Col-0 is associated with their rapid turnover. This mRNA cohort can include both direct and indirect targets of RHs. Group 2 ($n = 487$) mRNAs decayed more rapidly in the triple mutant (*rh6812* $t_{1/2}$ < Col-0 $t_{1/2}$), while group 3 mRNAs were unaffected ($n = 8,261$; *rh6812* $t_{1/2} \simeq$ Col-0 $t_{1/2}$).

The RH substrates (group 1) had characteristics that provide insights into RH function and biological relevance. First, these collectively had the shortest half-lives in Col-0 of the three groups (Fig. 4c). The median Col-0 $t_{1/2}$ of group 1 mRNAs was 108 min whereas that of groups 2 and 3 was 263 and 299 min, respectively. Second, the RH substrates had fewer codons, typically fewer introns and were shorter than non-substrate mRNAs, whereas their 5′ and 3′ untranslated region lengths showed no overall difference (Supplementary Fig. 10a,b). Third, the RH substrate GO functions encompassed a wide range of biological processes (Supplementary Table 5). Of these, 1,294 (17.8%) are involved in stress and immune responses (Fig. 4d). These stress-response mRNAs include disease-resistance proteins, transcription factors and signalling proteins such as kinases (Supplementary Table 6).

Since all three RHs co-localize with DCP2 and VCS, we hypothesized that their substrates are degraded in a decapping-dependent manner. A parallel decay experiment was performed in the decapping mutant *vcs-7* (ref. [7]), and co-analysis of *rh6812* and *vcs-7* effects on decay identified 5,832 out of 6,941 RH substrates (84%) as VCS substrates (Fig. 4e). The analysis also identified RH- and VCS-specific substrates. Comparison of 1,247 stress-response RH substrates to those dependent on VCS revealed that the majority (1,027, 82.4%) require VCS and are therefore degraded by the

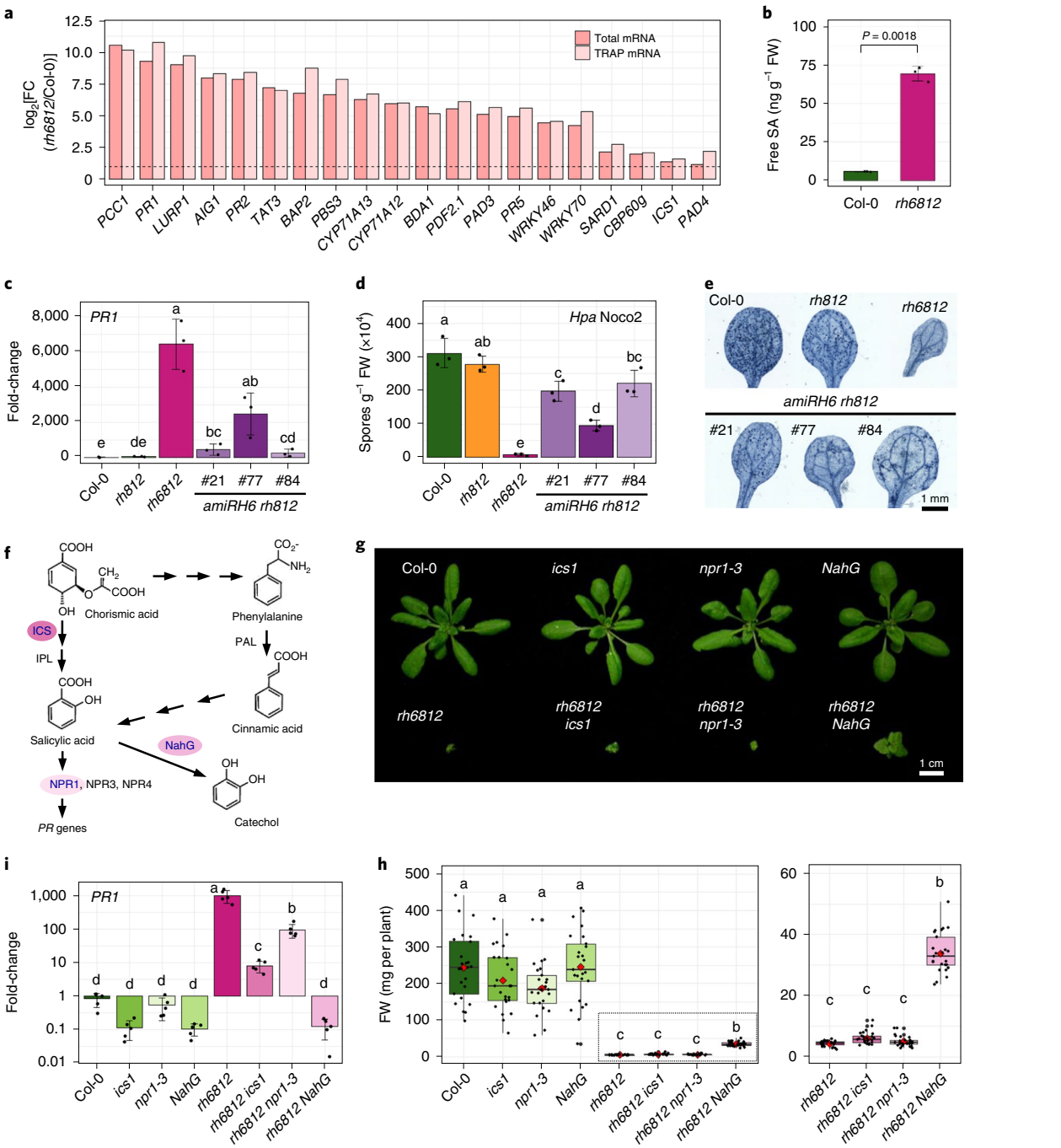

Fig. 6 | The triple *rh6812* mutant exhibits a constitutive immune response. a, Examples of defence-related genes with constitutively elevated transcripts in *rh6812*. Data are presented as $\log_2$[FC] of total and TRAP mRNA abundance in *rh6812* relative to Col-0. Horizontal dashed line, $\log_2$[FC] = 1. **b**, SA content in 7-day-old seedlings of *rh6812* in comparison to Col-0. Error bars, s.d. ($n = 3$); two-sided Welch's two-sample *t*-test. **c**, Quantitative PCR with reverse transcription (RT-qPCR) of *PR1* transcripts in 7-day-old seedlings ($n = 3$) of Col-0, *rh812*, *rh6812* and *amiRH6 rh812* lines. FC calculated using *Actin 1* (*ACT1*) as reference. Error bars, s.d. ($n = 3$). **d**, Quantification of *Hpa* Noco2 sporulation on seedlings ($n = 3$ per genotype). **e**, Representative cotyledons stained with lactophenol trypan blue at 7 days after inoculation. The experiment in **d**,**e** was repeated twice with similar results. **f**, Diagram of SA biosynthesis, perception and degradation. **g**, Representative rosette growth phenotype of 28-day-old plants—Col-0, single *ics1* and *npr1-3* mutants, Col-0 overexpressing the bacterial *NahG*, triple *rh6812* mutant, quadruple *rh6812 ics1* and *rh6812 npr1-3* mutants, and triple *rh6812* mutant combined with *NahG*. **h**, Fresh weight of 28-day-old plants ($n = 25$) of genotypes presented in **g**. Boxplot boundaries represent the first and third quartiles; a horizontal line divides the interquartile range, median; red diamonds, mean. **i**, RT-qPCR quantitation of *PR1* transcript levels in 7-day-old seedlings of genotypes presented in **g**. Relative transcript fold change calculated using *ACT1* as reference. Error bars, s.d. ($n = 5$). Means significantly different between genotypes in **c**,**d**,**h**,**i** are indicated by different letters; **h**,**i**, data were log-transformed ($P < 0.05$, ANOVA with Tukey's HSD test). **c**,**d**,**h**,**i**, See Source Data for *P* values. FW, fresh weight.

decapping pathway (Fig. 4f). The RH substrates had a shorter $t_{1/2}$, whether or not they require VCS, as compared to those requiring only VCS, or neither RHs nor VCS, for decay (Fig. 4g). These results verify that the majority of mRNAs targeted by RHs are ephemeral targets of 5′-to-3′ turnover, and provide further evidence that RHs accelerate the decay of these mRNAs.

Stress-related mRNAs are stabilized and preferentially ribosome-loaded in the *rh6812* genotype. We also considered whether steady-state abundance and translation of RH substrates were altered in *rh6812* seedlings relative to Col-0. A meta-analysis of the combined mRNA decay, transcriptome and translatome datasets revealed that of all mRNAs with higher levels in *rh6812* total and TRAP mRNA populations, 42% (383) were RH substrates (Fig. 5a). A homodirectional increase in steady-state and polysomal mRNA abundance was expected, but the 383 RH substrates also had a significantly higher translational status than the 522 RH-independent mRNAs from this group (Fig. 5b). This indicates that increased stability and abundance of these RH substrates are coupled with their preferential ribosome association in the *rh6812* genotype, which was not evident for the full cohort of RH substrates. GO enrichment analysis revealed that the 383-mRNA cohort is enriched for transcripts encoding stress/defence-response proteins (Supplementary Table 7). The decay kinetics for eight representative defence genes (Fig. 5c) support the conclusion that these RH substrates are synthesized at a basal level but are rapidly degraded under standard growth conditions.

The *rh6812* mutant phenotype is associated with auto-immunity. The observation that aseptically grown *rh6812* seedlings stabilize and over-acumulate mRNAs involved in defence response led us to hypothesize that the diminutive mutant phenotype results from a constitutive immune response. The most ectopically elevated mRNAs in *rh6812* included those of many well-known defence-response genes (Fig. 6a). Moreover, levels of the defence phytohormone salicylic acid (SA) were significantly elevated in *rh6812* relative to Col-0 seedlings (Fig. 6b), consistent with increased levels of *ISOCHORISMATE SYNTHASE 1* (*ICS1*) mRNA encoding a key enzyme in SA biosynthesis (Fig. 6a). Transcript levels of the SA-responsive, defence-response marker *PATHOGENESIS-RELATED 1* (*PR1*) were also significantly elevated in *amiRH6 rh812* lines, but to lower levels than in *rh6812* seedlings (Fig. 6c). Both *amiRH6 rh812* and *rh6812* seedlings were more resistant to the pathogenic Noco2 isolate of the oomycete *Hyaloperonospora arabidopsidis* than Col-0, with the *rh6812* genotype showing the highest level of resistance (Fig. 6d,e).

Auto-immunity was demonstrated in the mRNA decay mutants *up-frameshift 1* (*upf1*)[31] and *pat1* (ref. [14]). Their auto-immune phenotypes can be uncoupled by inactivation of the immune regulator ENHANCED DISEASE SUSCEPTIBILITY 1 (EDS1) and/or PHYTOALEXIN DEFICIENT 4 (PAD4)[14,19]. These lipase-like proteins constitute key signalling components in effector-triggered immunity and basal disease resistance[32,33]. We found that *PAD4* transcripts were stabilized with concomitant elevation in total and TRAP mRNA abundance, as well as translation status in *rh6812* seedlings (Figs. 5d and 6a). This coincided with the elevation of known EDS1/PAD4-inducible mRNAs[33] in the transcriptome and translatome of *rh6812* (Extended Data Fig. 7a). However, based on phenotypic analyses and quantification of *PR1* transcripts and SA levels in the quadruple mutants *rh6812 eds1-2* and *rh6812 pad4-1* (Extended Data Fig. 7b–e), the constitutive immunity exhibited by *rh6812* is partially dependent on PAD4 but not EDS1 function.

Because *rh6812* seedlings over-acumulate SA, we tested whether manipulation of SA synthesis, perception or catabolism would rescue the *rh6812* phenotypes. This included combining *rh6812* with mutations of *ICS1* and *NONEXPRESSER OF PR GENES 1* (*NPR1*) that encodes a SA receptor, and with ectopic expression of the bacterial salicylate hydroxylase NahG that converts SA into catechol (Fig. 6f). Although the homozygous *rh6812 ics1* and *rh6812 npr1-3* genotypes were as diminutive as the triple mutant, *NahG* partially rescued *rh6812* rosette growth (Fig. 6g,h). This rescue was accompanied by a significant reduction in *PR1* transcripts in *rh6812 NahG* seedlings, to levels indistinguishable from control genotypes Col-0, *ics1*, *npr1-3* and *NahG* (Fig. 6i). *PR1* transcript levels were reduced in *rh6812 ics1* and *rh6812 npr1-3* relative to *rh6812* seedlings, but remained significantly higher than in the control genotypes. We conclude that severe RH deficiency promotes a SA-mediated immune response that contributes to the dampening of growth in *rh6812*. Collectively, these data uncover a functional role of RHs in limiting the basal accumulation of transcripts associated with innate immunity.

Discussion

The *Arabidopsis* DHH1/DDX6-like proteins RH6, RH8 and RH12 are integral to growth and development, with the triple *rh6812* mutant showing pleiotropic phenotypes with some overlap with other mRNA decapping mutants. When expressed under the control of their native promoters, all three RHs localize to the nucleus and cytoplasm, consistent with previous analyses using ectopic expression[34–36]. SGs and PBs are the two major conserved translationally repressed mRNP complexes in the cytoplasm of eukaryotic cells, with PBs typically associated with translational repression and 5′ decapping-dependent decay[37,38]. In the root meristematic region of seedlings, RHs form inducible mRNP complexes that overlap with one another and with the PB markers DCP2 and VCS and the SG marker UBP1C. Consistent with this finding, RH6 interacts with the translational repressor and decapping activator DCP5, while all three RHs co-immunoprecipitate with the nonsense-mediated decay factor UPF1, along with the core decapping activators DCP1 and VCS, the eukaryotic translation initiation factor eIF4G and several poly(A)-binding proteins[35].

We found that RHs and PB and SG markers are not uniformly overlapping, strengthening the notion that these complexes are heterogeneous. Our demonstration that RHs are required for the formation of visible DCP2 and VCS foci suggests that these helicases contribute to PB assembly and dynamics, as demonstrated for DHH1/DDX6 proteins in other organisms[23,39–41]. It remains elusive as to how RHs contribute to the formation of DCP2 and VCS assemblies, while only a subset of them overlap with RHs. In addition to PBs, RHs may contribute to the formation of stress-induced UBP1C SGs, as observed in yeast DHH1 (ref. [29]), although this might be lineage specific because depletion of DDX6 in human HeLa cells does not affect SG formation[39].

In *Arabidopsis*, the depletion of PBs in the *dcp5-1* mutant results in precocious translation of specific mRNAs in etiolated seedlings[42]. Here we found that reduction of PBs in light-grown *rh6812* seedlings is associated with ectopic elevation of the steady-state abundance and coincident ribosome association of stress- and defence-response mRNAs. This suggests that the role of PBs in translational repression may include the control of stress-related mRNAs under non-stress conditions. Furthermore, our global RNA decay analysis showed that the turnover of thousands of short-lived mRNAs is compromised in *rh6812* seedlings. The co-localization and 84% overlap of RH and VCS substrates strongly support the conclusion that RHs are components of the decapping-dependent, 5′-to-3′ decay machinery. Comparison of RH and VCS substrates also supports the notion that mRNA decay does not necessarily occur in visible PBs, as their formation was impaired in *rh6812*, but the degradation of >3,800 VCS-specific substrates was unaffected. It is yet to be determined whether RH-assisted decay occurs in PBs of smaller than detectable size, or co-translationally on elongating ribosomes.

Plants have evolved diverse and intricate systems to rapidly sense and respond to environmental insults, including pathogens. While lacking adaptive immunity, plants have a battalion of immune receptors, including *R* genes that encode nucleotide-binding leucine-rich repeat (NLR) proteins to recognize different pathogen-derived effector proteins and trigger a robust defence response[43]. Since defence occurs at the expense of cellular energy reserves, immune-response

gene and protein activation must be tightly regulated to avoid auto-immunity and maintain plant growth. This includes NLR regulation that operates from epigenetic to post-translational levels[43,44]. Post-transcriptional control of *R* gene transcripts is multifaceted, including regulation of alternative splicing[45], alternative polyadenylation[46], small RNA-mediated silencing[47], nonsense-mediated decay[19] and translation[48]. The dysregulation of any of these processes often causes a sensitized or constitutive immune response.

There is compelling evidence that general cytoplasmic mRNA decay contributes to the control of the defence response in *Arabidopsis*. Pattern-triggered immunity activates decapping-dependent turnover of transcripts known to decline in response to the elicitor flg22 (ref. [49]), although the effect on global decay is unknown. Moreover, the decapping mutant *pat1* exhibits an auto-immune phenotype that is suppressed by mutations of the NLR SUPPRESSOR OF MKK1 MKK2 2 (SUMM2) and the defence regulator EDS1 (ref. [14]). In yeast, PAT1 interacts with DHH1 to repress translation and activate mRNA decapping[26,50]. Similar to *pat1*, the triple *rh6812* mutant exhibits auto-immunity, albeit in an EDS1-independent manner. Our mRNA decay analysis identified 44 annotated *R* gene transcripts along with 1,250 other stress- and defence-response mRNAs, including those encoding plant-specific transcription factors that are stabilized in the *rh6812* genotype. Many of these mRNAs increase in translational status in concert with elevated stability and abundance. This indicates that RHs actively repress basal or aberrant activation of the plant immune response. We hypothesize that the DHH1/DDX6-like protein family plays a conserved role as a negative regulator of innate immunity in eukaryotes, because the depletion of human DDX6 induces global upregulation of interferon-stimulated and other immune genes in the absence of infection[51]. The deficiency in RH activity is accompanied by a reduction in plant growth, reminiscent of genotypes with constitutive innate immunity[52]. While the *rh6812* phenotype is partially rescued when the ectopic accumulation of the key defence metabolite SA is controlled, we cannot exclude the role of stabilized mRNAs unrelated to SA production in the reduction of rosette growth, given that RH substrates encompass diverse stress-response mRNAs and that RH deficiency shifts the balance of stress- and growth-related transcripts.

In summary, a severe deficiency of RH function results in catastrophic alteration of seedling mRNA homeostasis, allowing the accumulation and translation of stress- and defence-response transcripts while dampening mRNAs important for growth and development. The regulation of mRNA turnover is integral to rapid changes in gene expression in response to stress[53]. This study illuminates the substantial contribution of mRNA decay in shaping the cellular transcriptome and translatome under optimal conditions. The findings raise the notion that stress-responsive transcripts are constitutively synthesized at a basal level, but that their accumulation and translation are limited by degradation. Inhibition of the decay machinery, in conjunction with activation of their transcription above the basal level, would allow a rapid and robust response to stress. This raises new questions as to whether RH function is dynamically modulated to allow stress-response transcripts to escape destabilization in response to cues that activate their transcription to provide pathogen resistance or stress resilience.

Methods

Further details are provided in the Supplementary Information.

Reporting Summary. Further information on research design is available in the Nature Research Reporting Summary linked to this article.

Data availability

Sequence data are deposited in GEO accession no. GSE136713. All other data needed to evaluate the conclusions are in the Supplementary Information. Source Data for Figs. 1, 2 and 6, and Extended Data Figs. 2–5 and 7 are provided with the paper. Sequence Read Archive, http://www.ncbi.nlm.nih.gov/sra; NCBI Gene Expression Omnibus, https://www.ncbi.nlm.nih.gov/geo/.

Received: 17 September 2019; Accepted: 29 April 2020;
Published online: 01 June 2020

References

1. Chantarachot, T. & Bailey-Serres, J. Polysomes, stress granules, and processing bodies: a dynamic triumvirate controlling cytoplasmic mRNA fate and function. *Plant Physiol.* **176**, 254–269 (2018).
2. Sheth, U. & Parker, R. Decapping and decay of messenger RNA occur in cytoplasmic processing bodies. *Science* **300**, 805–808 (2003).
3. Hubstenberger, A. et al. P-body purification reveals the condensation of repressed mRNA regulons. *Mol. Cell* **68**, 144–157 (2017).
4. Sorenson, R. & Bailey-Serres, J. Selective mRNA sequestration by OLIGOURIDYLATE-BINDING PROTEIN 1 contributes to translational control during hypoxia in *Arabidopsis*. *Proc. Natl Acad. Sci. USA* **111**, 2373–2378 (2014).
5. Merret, R. et al. Heat-shock protein HSP101 affects the release of ribosomal protein mRNAs for recovery after heat shock. *Plant Physiol.* **174**, 1216–1225 (2017).
6. Zhang, W., Murphy, C. & Sieburth, L. E. Conserved RNase II domain protein functions in cytoplasmic mRNA decay and suppresses *Arabidopsis* decapping mutant phenotypes. *Proc. Natl Acad. Sci. USA* **107**, 15981–15985 (2010).
7. Sorenson, R. S., Deshotel, M. J., Johnson, K., Adler, F. R. & Sieburth, L. E. *Arabidopsis* mRNA decay landscape arises from specialized RNA decay substrates, decapping-mediated feedback, and redundancy. *Proc. Natl Acad. Sci. USA* **115**, E1485–E1494 (2018).
8. Siwaszek, A., Ukleja, M. & Dziembowski, A. Proteins involved in the degradation of cytoplasmic mRNA in the major eukaryotic model systems. *RNA Biol.* **11**, 1122–1136 (2014).
9. Nagarajan, V. K., Jones, C. I., Newbury, S. F. & Green, P. J. XRN 5′→3′ exoribonucleases: structure, mechanisms and functions. *Biochimica Biophys. Acta Gene Regul. Mech.* **1829**, 590–603 (2013).
10. Xu, J., Yang, J.-Y., Niu, Q.-W. & Chua, N.-H. *Arabidopsis* DCP2, DCP1, and VARICOSE form a decapping complex required for postembryonic development. *Plant Cell* **18**, 3386–3398 (2006).
11. Goeres, D. C. et al. Components of the *Arabidopsis* mRNA decapping complex are required for early seedling development. *Plant Cell* **19**, 1549–1564 (2007).
12. Xu, J. & Chua, N.-H. *Arabidopsis* decapping 5 is required for mRNA decapping, P-body formation, and translational repression during postembryonic development. *Plant Cell* **21**, 3270–3279 (2009).
13. Perea-Resa, C. et al. LSM proteins provide accurate splicing and decay of selected transcripts to ensure normal *Arabidopsis* development. *Plant Cell* **24**, 4930–4947 (2012).
14. Roux, M. E. et al. The mRNA decay factor PAT1 functions in a pathway including MAP kinase 4 and immune receptor SUMM2. *EMBO J.* **34**, 593–608 (2015).
15. Martínez de Alba, A. E. et al. In plants, decapping prevents RDR6-dependent production of small interfering RNAs from endogenous mRNAs. *Nucleic Acids Res.* **43**, 2902–2913 (2015).
16. Xu, J. & Chua, N.-H. Dehydration stress activates *Arabidopsis* MPK6 to signal DCP1 phosphorylation. *EMBO J.* **31**, 1975–1984 (2012).
17. Soma, F. et al. ABA-unresponsive SnRK2 protein kinases regulate mRNA decay under osmotic stress in plants. *Nat. Plants* **3**, 16204 (2017).
18. Perea-Resa, C. et al. The LSM1-7 complex differentially regulates *Arabidopsis* tolerance to abiotic stress conditions by promoting selective mRNA decapping. *Plant Cell* **28**, 505–520 (2016).
19. Gloggnitzer, J. et al. Nonsense-mediated mRNA decay modulates immune receptor levels to regulate plant antibacterial defense. *Cell Host Microbe* **16**, 376–390 (2014).
20. Presnyak, V. & Coller, J. The DHH1/RCKp54 family of helicases: an ancient family of proteins that promote translational silencing. *Biochimica Biophys. Acta Gene Regul. Mech.* **1829**, 817–823 (2013).
21. Kami, D. et al. The DEAD-box RNA-binding protein DDX6 regulates parental RNA decay for cellular reprogramming to pluripotency. *PLoS ONE* **13**, e0203708 (2018).
22. Boag, P. R., Atalay, A., Robida, S., Reinke, V. & Blackwell, T. K. Protection of specific maternal messenger RNAs by the P body protein CGH-1 (Dhh1/RCK) during *Caenorhabditis elegans* oogenesis. *J. Cell Biol.* **182**, 543–557 (2008).
23. Kamenska, A. et al. The DDX6-4E-T interaction mediates translational repression and P-body assembly. *Nucleic Acids Res.* **44**, 6318–6334 (2016).
24. Wang, M. et al. ME31B globally represses maternal mRNAs by two distinct mechanisms during the *Drosophila* maternal-to-zygotic transition. *eLife* **6**, e27891 (2017).
25. Coller, J. M., Tucker, M., Sheth, U., Valencia-Sanchez, M. A. & Parker, R. The DEAD box helicase, Dhh1p, functions in mRNA decapping and interacts with both the decapping and deadenylase complexes. *RNA* **7**, 1717–1727 (2001).

26. Coller, J. & Parker, R. General translational repression by activators of mRNA decapping. *Cell* **122**, 875–886 (2005).
27. Radhakrishnan, A. et al. The DEAD-box protein Dhh1p couples mRNA decay and translation by monitoring codon optimality. *Cell* **167**, 122–132 (2016).
28. Zhang, X. et al. Suppression of endogenous gene silencing by bidirectional cytoplasmic RNA decay in *Arabidopsis*. *Science* **348**, 120–123 (2015).
29. Hondele, M. et al. DEAD-box ATPases are global regulators of phase-separated organelles. *Nature* **573**, 144–148 (2019).
30. Mustroph, A. et al. Profiling translatomes of discrete cell populations resolves altered cellular priorities during hypoxia in *Arabidopsis*. *Proc. Natl Acad. Sci. USA* **106**, 18843–18848 (2009).
31. Riehs-Kearnan, N., Gloggnitzer, J., Dekrout, B., Jonak, C. & Riha, K. Aberrant growth and lethality of *Arabidopsis* deficient in nonsense-mediated RNA decay factors is caused by autoimmune-like response. *Nucleic Acids Res.* **40**, 5615–5624 (2012).
32. Feys, B. J., Moisan, L. J., Newman, M. A. & Parker, J. E. Direct interaction between the *Arabidopsis* disease resistance signaling proteins, EDS1 and PAD4. *EMBO J.* **20**, 5400–5411 (2001).
33. Cui, H. et al. A core function of EDS1 with PAD4 is to protect the salicylic acid defense sector in *Arabidopsis* immunity. *New Phytol.* **213**, 1802–1817 (2017).
34. Baek, W., Lim, C. W. & Lee, S. C. A DEAD-box RNA helicase, RH8, is critical for regulation of ABA signalling and the drought stress response via inhibition of PP2CA activity. *Plant Cell Environ.* **41**, 1593–1604 (2018).
35. Chicois, C. et al. The UPF1 interactome reveals interaction networks between RNA degradation and translation repression factors in *Arabidopsis*. *Plant J.* **96**, 119–132 (2018).
36. Sulkowska, A. et al. RNA helicases From the DEA(D/H)-box family contribute to plant NMD efficiency. *Plant Cell Physiol.* **61**, 144–157 (2019).
37. Protter, D. S. W. & Parker, R. Principles and properties of stress granules. *Trends Cell Biol.* **26**, 668–679 (2016).
38. Luo, Y., Na, Z. & Slavoff, S. A. P-bodies: composition, properties, and functions. *Biochemistry* **57**, 2424–2431 (2018).
39. Serman, A. et al. GW body disassembly triggered by siRNAs independently of their silencing activity. *Nucleic Acids Res.* **35**, 4715–4727 (2007).
40. Minshall, N., Kress, M., Weil, D. & Standart, N. Role of p54 RNA helicase activity and its C-terminal domain in translational repression, P-body localization and assembly. *Mol. Biol. Cell* **20**, 2464–2472 (2009).
41. Ayache, J. et al. P-body assembly requires DDX6 repression complexes rather than decay or Ataxin2/2L complexes. *Mol. Biol. Cell* **26**, 2579–2595 (2015).
42. Jang, G.-J., Yang, J.-Y., Hsieh, H.-L. & Wu, S.-H. Processing bodies control the selective translation for optimal development of *Arabidopsis* young seedlings. *Proc. Natl Acad. Sci. USA* **116**, 6451–6456 (2019).
43. Borrelli, G. M. et al. Regulation and evolution of NLR genes: a close interconnection for plant immunity. *Int. J. Mol. Sci.* **19**, 1662 (2018).
44. Lai, Y. & Eulgem, T. Transcript-level expression control of plant NLR genes. *Mol. Plant Pathol.* **19**, 1267–1281 (2018).
45. Zhang, X.-N. et al. Transcriptome analyses reveal SR45 to be a neutral splicing regulator and a suppressor of innate immunity in *Arabidopsis thaliana*. *BMC Genomics* **18**, 772 (2017).
46. Tsuchiya, T. & Eulgem, T. An alternative polyadenylation mechanism coopted to the *Arabidopsis* RPP7 gene through intronic retrotransposon domestication. *Proc. Natl Acad. Sci. USA* **110**, E3535–E3543 (2013).
47. Boccara, M. et al. The *Arabidopsis* miR472-RDR6 silencing pathway modulates PAMP- and effector-triggered immunity through the post-transcriptional control of disease resistance genes. *PLoS Pathog.* **10**, e1003883 (2014).
48. Wu, Z. et al. Regulation of plant immune receptor accumulation through translational repression by a glycine-tyrosine-phenylalanine (GYF) domain protein. *eLife* **6**, e23684 (2017).
49. Yu, X. et al. Orchestration of processing body dynamics and mRNA decay in *Arabidopsis* Immunity. *Cell Rep.* **28**, 2194–2205 (2019).
50. Sharif, H. et al. Structural analysis of the yeast Dhh1-Pat1 complex reveals how Dhh1 engages Pat1, Edc3 and RNA in mutually exclusive interactions. *Nucleic Acids Res.* **41**, 8377–8390 (2013).
51. Lumb, J. H. et al. DDX6 represses aberrant activation of interferon-stimulated genes. *Cell Rep.* **20**, 819–831 (2017).
52. van Wersch, R., Li, X. & Zhang, Y. Mighty dwarfs: *Arabidopsis* autoimmune mutants and their usages in genetic dissection of plant immunity. *Front. Plant Sci.* **7**, 1717 (2016).
53. Arribere, J. A., Doudna, J. A. & Gilbert, W. V. Reconsidering movement of eukaryotic mRNAs between polysomes and P bodies. *Mol. Cell* **44**, 745–758 (2011).

Acknowledgements

We thank J. Parker for kindly providing *eds1-2* and *pad4-1* seeds, M. Crespi for *rdr6*$^{sgs2\text{-}1}$ and *sgs3-1* and Y. Watanabe for *proDCP2:DCP2-GFP* in *dcp2-1*. We thank C. Bousquet-Antonelli for sharing RH6/8/12 antisera. We thank the members of the Bailey-Serres and Sieburth laboratories for discussion. This research was supported by the United States National Science Foundation (grant nos. MCB-1021969 to J.B.-S. and L.E.S. and MCB-1716913 to J.B.-S.) and a UC MacArthur Foundation Chair award to J.B.-S. T.C. was supported by a Royal Thai Government Development and Promotion of Science and Technology Talents Project scholarship.

Author contributions

T.C., R.S.S., L.S. and J.B.-S. conceived and designed experiments. T.C., R.S., M.H., H.K., A.T.K. and K.A. performed experiments. D.C. contributed to the preparation of genetic material. K.D., T.E., L.S. and J.B.-S. provided reagents. T.C., R.S.S., M.H., L.S. and J.B.-S. analysed data. T.C., R.S.S., L.S. and J.B.-S. wrote the manuscript.

Competing interests

The authors declare no competing interests.

Additional information

Extended data is available for this paper at https://doi.org/10.1038/s41477-020-0681-8.

Supplementary information is available for this paper at https://doi.org/10.1038/s41477-020-0681-8.

Correspondence and requests for materials should be addressed to J.B.-S.

Peer review information *Nature Plants* thanks Yuichiro Watanabe and the other, anonymous, reviewers for their contribution to the peer review of this work.

Reprints and permissions information is available at www.nature.com/reprints.

Publisher's note Springer Nature remains neutral with regard to jurisdictional claims in published maps and institutional affiliations.

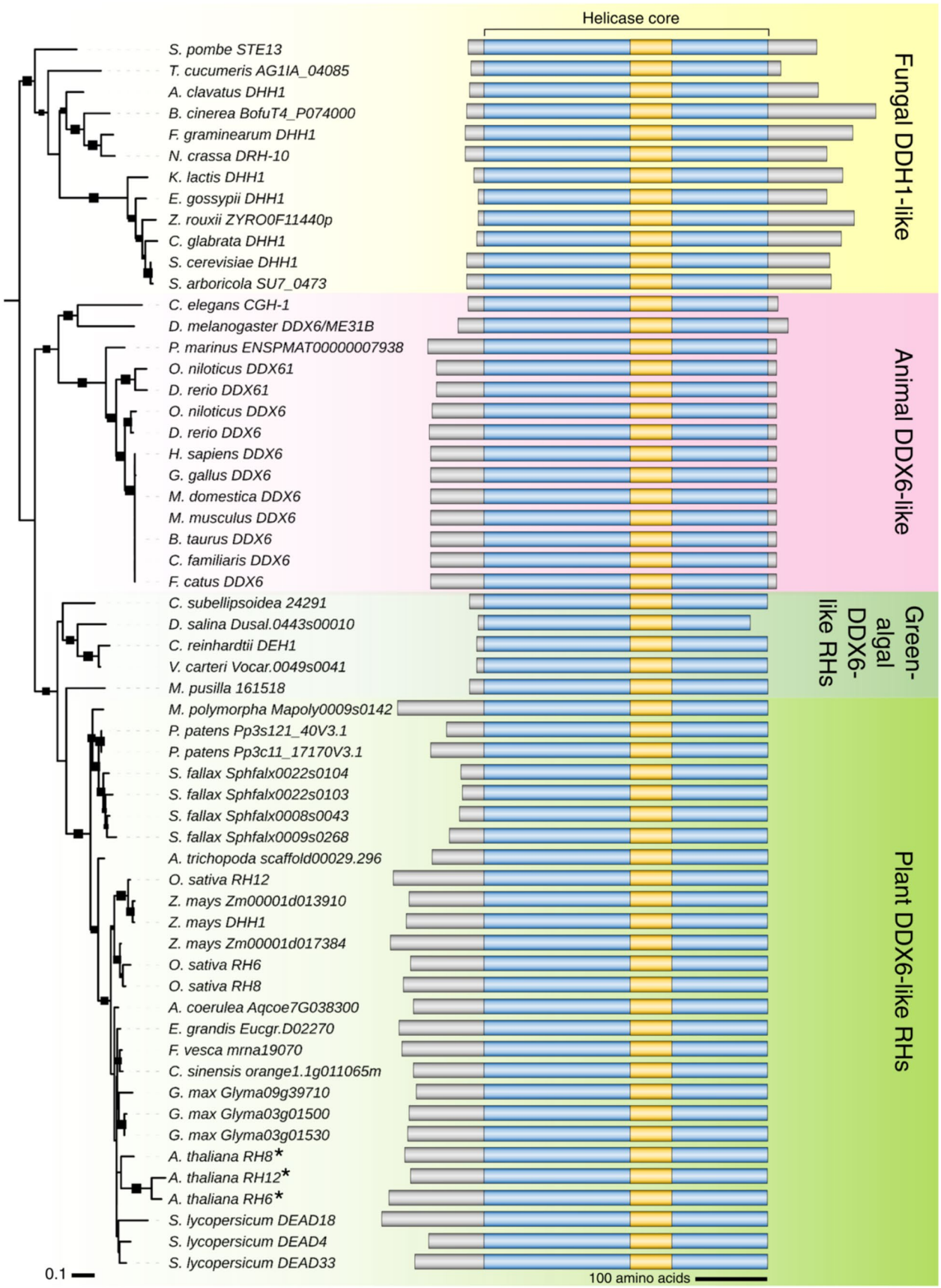

Extended Data Fig. 1 | See next page for caption.

Extended Data Fig. 1 | Phylogenetic relationship and schematic representation of the primary sequence structure of eukaryotic DHH1/DDX6-like DEAD-box RNA helicases. The evolutionary history was inferred from 58 representative DHH1/DDX6-like helicases across different eukaryotic lineages. The sequences were aligned using the Muscle algorithm, and the phylogenetic tree was generated with the Maximum Likelihood method with 1000 bootstrap replicates. Evolutionary rate differences among sites were modeled with a discrete Gamma distribution. The tree is shown to scale, with branch lengths measured as the number of substitutions per site. Black rectangular boxes on the tree branches depict bootstrap values greater than 50%, with the size of the boxes proportional to the bootstrap values. Grey boxes represent the N- and C-terminal extensions; blue boxes, RecA-like domains; yellow boxes, linker regions.

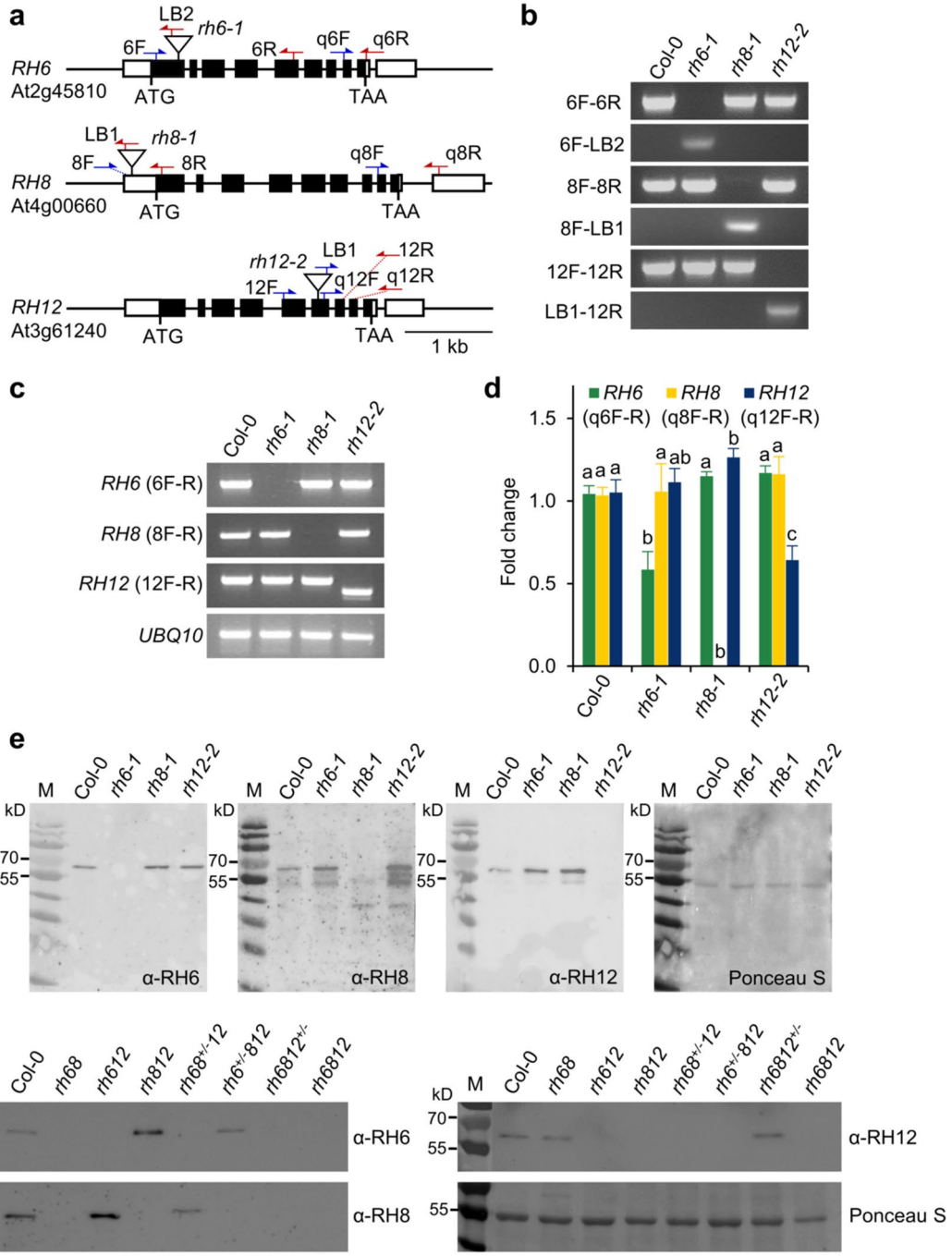

Extended Data Fig. 2 | Characterization of Arabidopsis *rh6-1*, *rh8-1* and *rh12-2* mutants and their higher-order mutant combinations. a, Schematic representation of the *RH6*, *RH8* and *RH12* loci and their associated T-DNA insertion alleles. Untranslated and coding regions are depicted as white and black boxes, respectively. Introns are depicted as lines. 'ATG' and 'TAA' indicate the translational initiation and stop codon, respectively. Inverted white triangles refer to the positions of T-DNA insertions in the *rh6-1*, *rh8-1* and *rh12-2* alleles. Arrows indicate the orientation and approximate position of primers used for molecular genotyping of the genes or the T-DNAs: blue, forward primers; red, reverse primers. **b**, PCR-based genotyping of the homozygous *rh6-1*, *rh8-1* and rh*12-2* alleles. Gene and T-DNA-specific primers represented in **a** were used for PCR amplification of genomic DNA from Col-0 and homozygous *rh6-1*, *rh8-1* and *rh12-2* insertion alleles. Results validated with other primers. **c**, Reverse transcriptase (RT)-PCR analysis of *RH6*, *RH8* and *RH12* transcripts. Primers flanking the T-DNAs as indicated in **a** were used for PCR-based specific detection of *RH6*, *RH8* and *RH12* transcripts from the homozygous *rh6-1*, *rh8-1* and rh*12-2* alleles in comparison to Col-0. *UBQ10* was used as an internal control. **d**, RT-qPCR analysis of *RH6*, *RH8* and *RH12* transcript levels in 7-day-old seedlings of the homozygous *rh6-1*, *rh8-1* and *rh12-2* mutants. Gene-specific primers located downstream of the T-DNA as indicated in **a** were used. Relative transcript fold-change was calculated using *PP2AA2* as a reference. Error bars, s.d. ($n = 3$). Statistical significance was determined by ANOVA, followed by Tukey's HSD test. Means that are significantly different from each other ($P < 0.05$) are denoted by different letters. See Source Data for fold change and *P* values. **e**, Western blot analysis of RH6, RH8 and RH12 protein levels in 5-day-old seedlings of the homozygous *rh6-1*, *rh8-1* and *rh12-2* mutants. **f**, Western blot analysis of RH6, RH8 and RH12 protein levels in rosette leaves of 32-day-old plants in the double (*rh68*, *rh612* and *rh812*), double homozygous hemizygous (*rh6*$^{+/-}$*812*, *rh68*$^{+/-}$*12* and *rh6812*$^{+/-}$) and triple (*rh6812*) mutants. For **e,f**, each lane was loaded with an equal quantity of protein from a crude homogenate, RH specific antisera were used[20]. The molecular weight marker (M) ladder and Ponceau S staining as loading control were imaged in visible light. Data are representative of two experiments.

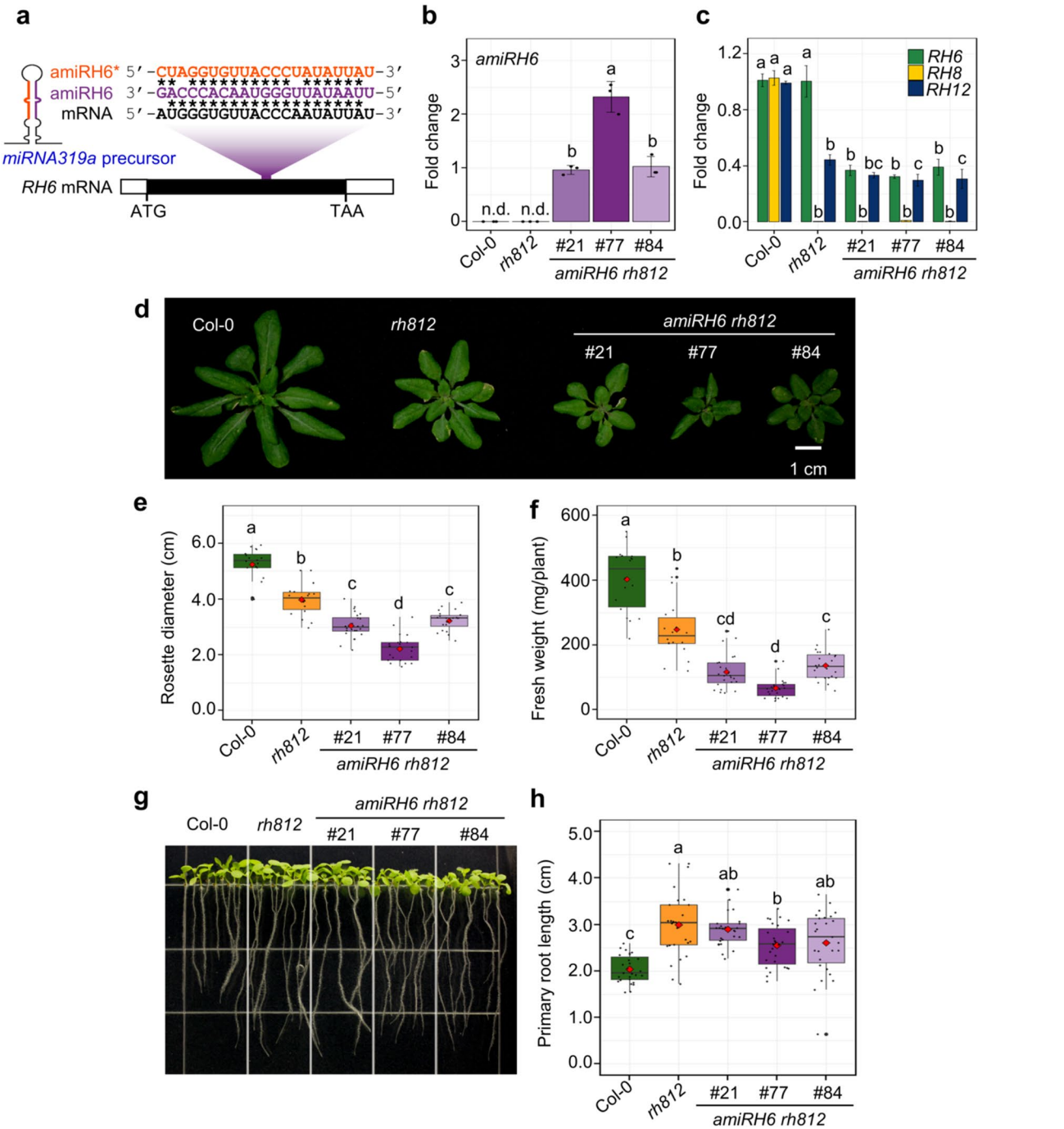

Extended Data Fig. 3 | Reduced expression of *RH6*, *RH8* and *RH12* affects plant growth. a, Schematic diagram and sequences of a 21-nucleotide artificial miRNA and its target site on *RH6* expressed in the Arabidopsis *MIR319a* backbone under the 35S promoter. **b**, Levels of the artificial *amiRH6* in 7-day-old seedlings of three independent *amiRH6* lines generated in *rh812* background (*amiRH6 rh812*) determined by pulsed stem-loop RT-qPCR. miRNA fold-change was calculated relative to line #21 using *U6* RNA as a reference. Error bars, s.d. ($n = 3$); n.d., not detectable. **c**, RT-qPCR analysis of *RH6*, *RH8* and *RH12* transcript levels in 7-day-old seedlings of Col-0, *rh812* and three *amiRH6 rh812* lines. Relative transcript fold-change was calculated using *PP2AA2* as a reference. Error bars, s.d. ($n = 3$). **d**, Representative rosette growth phenotype of 28-day-old plants of Col-0, *rh812* and the *amiRH6 rh812* lines. **e,, f**, Rosette diameters ($n = 24$) and fresh weights ($n = 18$-24) of 28-day-old plants of the genotypes presented in **d**. **g, h**, Phenotype (**g**) and primary root lengths (**h**, $n = 27$) of 7-day-old seedlings of the wild-type Col-0, the double *rh812* mutant and the *amiRH6 rh812* lines. Statistical significance was determined by ANOVA, followed by Tukey's HSD test. Means that are significantly different from each other ($P < 0.05$) are denoted by different letters. For **e**, **f** and **h**, boxplot boundaries represent the first and third quartiles; a horizontal line divides the interquartile range, median; red diamond, mean. See Source Data for exact sample sizes, fold change or *P* values for **b, c, e**, **f** and **h**.

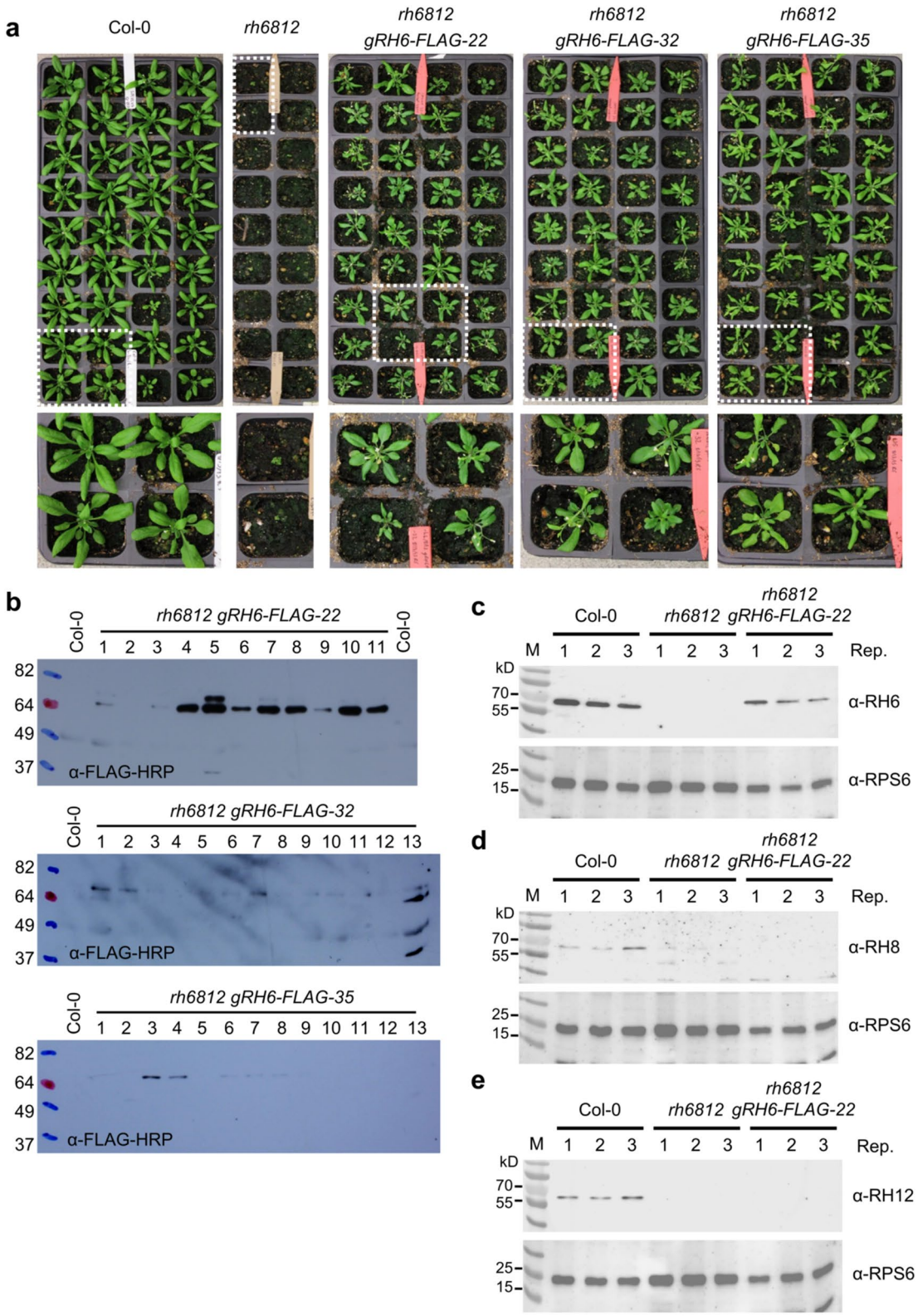

Extended Data Fig. 4 | Complementation of the *rh6812* phenotype by a genomic fragment of *RH6* with a C-terminal FLAG epitope tag (*gRH6-FLAG*). **a**, Rosette growth phenotype of three independent *rh6812 gRH6-FLAG* lines in the T2 population. 28-day-old plants are shown in comparison to the triple *rh6812* mutant and the wild-type Col-0. The *rh6812* genotype does not flower (0/36 plants), whereas *rh6812 gRH6-FLAG* plants are fertile (36/36 plants). Lower panels are magnified images of framed areas in the upper panels. **b**, Western blot analysis of the RH6-FLAG protein in three independent *rh6812 gRH6-FLAG* lines presented in **a** using anti-FLAG M2 antibody. Numbers represent individual plants in the T2 population. **c-e**, RH6, RH8 and RH12 protein abundance in the *rh6812* and *rh6812 gRH6-FLAG-22* genotypes. Western blot analysis of RH6 (**c**, upper panel), RH8 (**d**, upper panel), RH12 (**c**, upper panel) and RPS6 (**a, b** and **c**, lower panel). Protein levels were determined in triplicate ($n=3$) in 5-day-old seedling tissues of Col-0 *pro35S:HF-GFP-RPL18* and *rh6812 pro35S:HF-GFP-RPL18* and 7-day-old seedling tissues of *rh6812 gRH6-FLAG-22* homozygotes. RH specific antisera were used. Data are representative of two experiments.

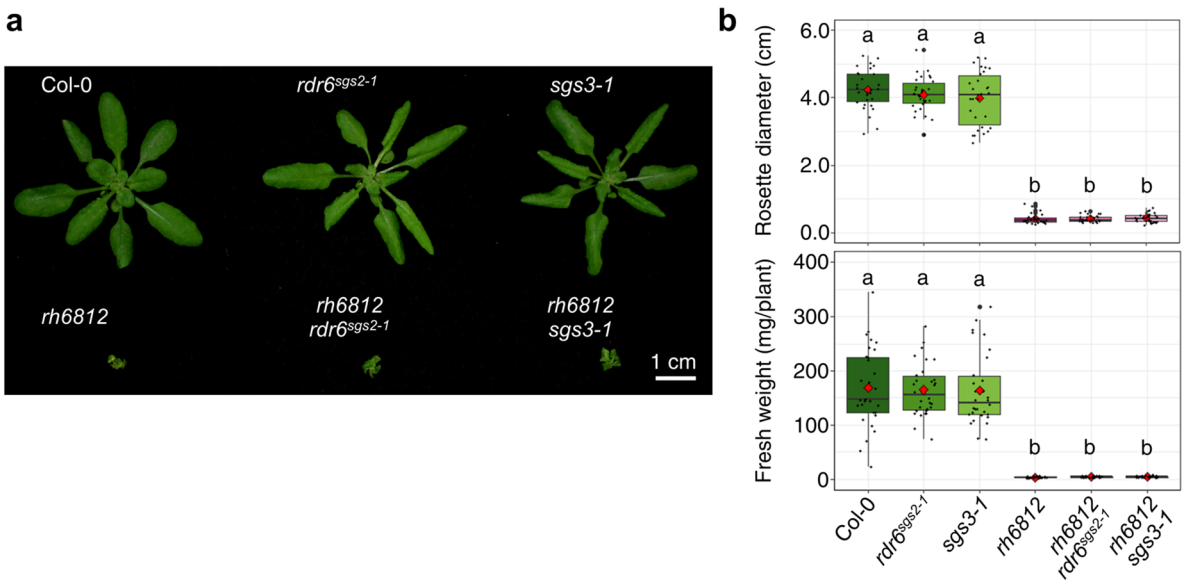

Extended Data Fig. 5 | The triple *rh6812* mutant phenotype is *RNA-DEPENDENT RNA POLYMERASE 6* and *SUPPRESSOR OF GENE SILENCING 3* independent. a, Representative rosette growth phenotype of 28-day-old plants of Col-0, single *rdr6*$^{sgs2\text{-}1}$ and *sgs3-1* mutants, triple *rh6812* mutant, and quadruple *rh6812 rdr6*$^{sgs2\text{-}1}$ and *rh6812 sgs3-1* mutants. **b**, Rosette diameter and fresh weight of 28-day-old plants of the genotypes presented in **a**. Boxplot boundaries represent the first and third quartiles; a horizontal line divides the interquartile range, median; red diamond, mean. Statistical significance was determined by ANOVA ($n = 30$), followed by Tukey's HSD test. Data were log-transformed. Means that are significantly different from one another ($P < 0.05$) are denoted by different letters. Data are representative of two experiments. See Source Data for *P* values.

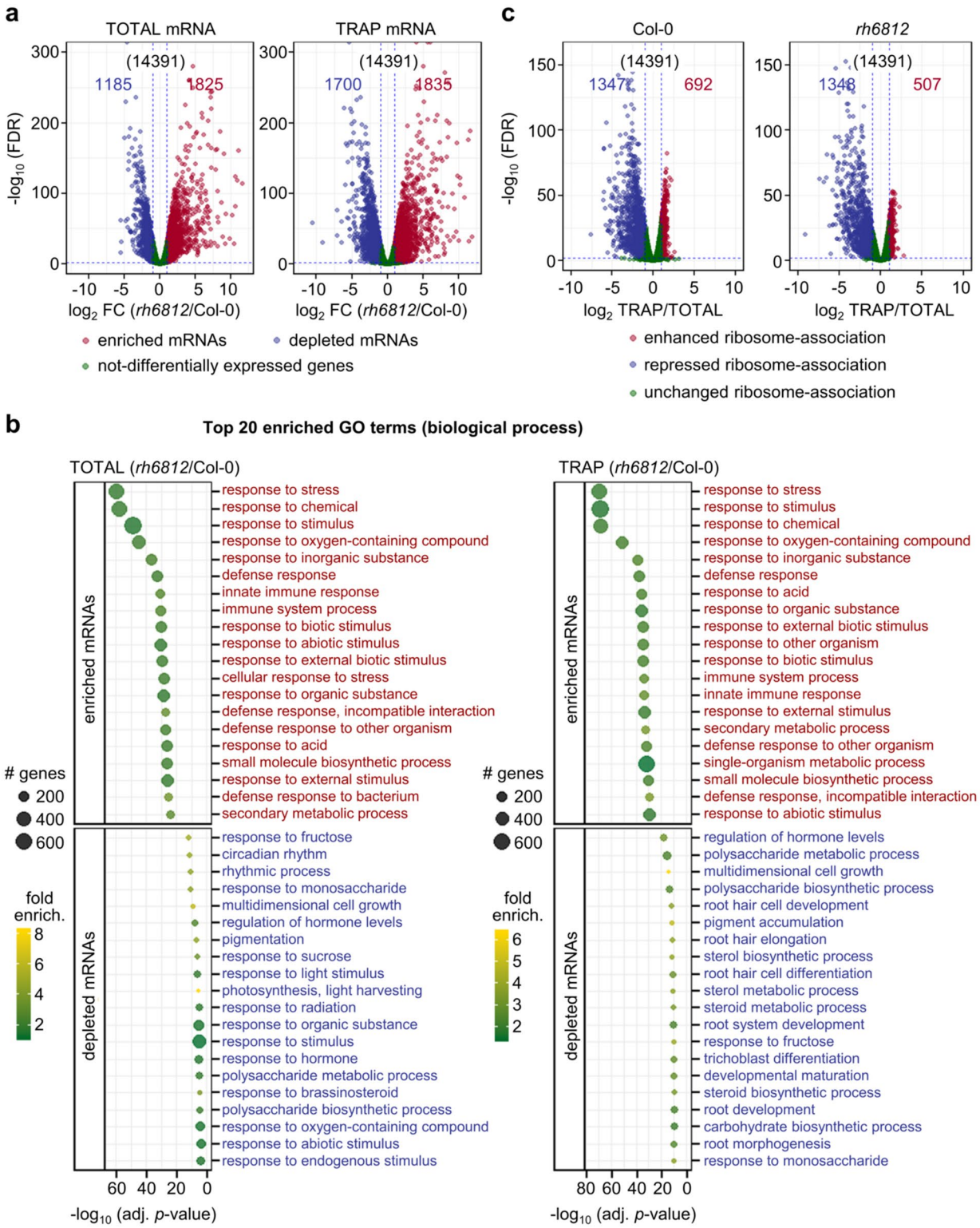

Extended Data Fig. 6 | The triple *rh6812* mutant transcriptome and translatome are enriched with stress/defense-responsive mRNAs but depleted of those required for growth and development. a, Volcano plots of change in Total and TRAP mRNA abundance of *rh6812* relative to Col-0 based on differential abundance analysis by edgeR. The $\log_2$ fold-change (FC) is shown on the x-axis, and the negative $\log_{10}$ of the false-discovery rate (FDR) is shown on the y-axis. Genes with $|\log_2 FC| \geq 1$ and FDR < 0.01 were considered differentially expressed. The total number of genes in the analysis is given in parentheses. **b**, GO functional categories (biological process) of gene transcripts enriched or depleted in *rh6812* relative to Col-0 as identified in **a**. Twenty non-redundant terms determined by a hypergeometric test with the lowest Bonferroni-adjusted *P* values presented. Fold enrichment (fold enrich.) represents the number of genes observed relative to the expected number in each category. **c**, Volcano plots of change in translational status calculated by comparison of steady-state Total and TRAP mRNA abundance in Col-0 and *rh6812* based on differential abundance analysis by edgeR. The $\log_2$ FC is shown on the x-axis, and the negative $\log_{10}$ of the FDR is shown on the *y*-axis. Genes with $|\log_2 FC| \geq 1$, FDR < 0.01 were considered enhanced or repressed ribosome-association. The total number of genes used in the analysis is presented in parentheses.

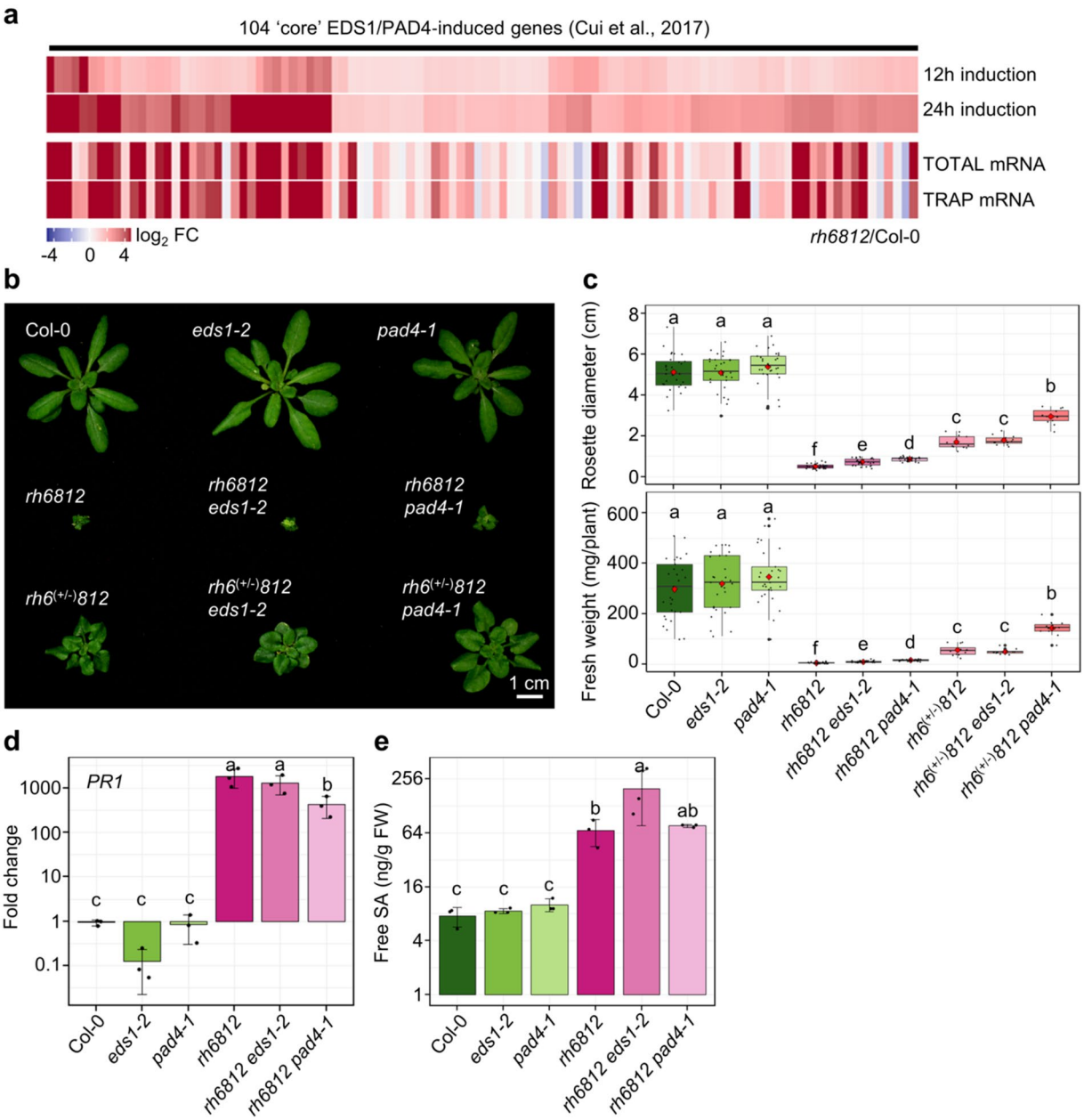

Extended Data Fig. 7 | The *rh6812* mutant exhibits autoimmunity in a PAD4-partially dependent but EDS1-independent manner. a, Heatmap representing relative fold change in Total and TRAP mRNA abundance for 104 'core' EDS1/PAD-induced genes[33] in *rh6812* relative to Col-0. Individual genes are presented as a column with the upper two rows showing their $\log_2$ FC following 12 and 24 hours of EDS1 and PAD4 overexpression[33], whereas the lower two rows representing their $\log_2$ FC in Total and TRAP populations of *rh6812* relative to Col-0. **b**, Representative rosette growth phenotype of 28-day-old plants of Col-0, *eds1-2*, *pad4-1*, *rh6812*, *rh6812 eds1-2*, *rh6812 pad4-1*, *rh6*$^{(+/-)}$*812*, *rh6*$^{(+/-)}$*812 eds1-2* and *rh6*$^{(+/-)}$*812 pad4-1* genotypes. **c**, Rosette diameter and fresh weight of 28-day-old plants ($n = 12$ or 30) of the genotypes presented in **b**. Boxplot boundaries represent the first and third quartiles; a horizontal line divides the interquartile range, median; red diamond, mean. **d**, RT-qPCR analysis of *PR1* transcripts in 7-day-old seedlings of the *rh6812 eds1-2* and *rh6812 pad4-1* genotypes relative to *rh6812* and the control genotypes Col-0, *eds1-2*, and *pad4-1*. Relative transcript fold-change was calculated using *ACT1* as a reference. Error bars, s.d. ($n = 3$). **e**, Comparison of SA levels in 7-day-old seedlings of the genotypes as in **d**. Error bars, s.d. ($n = 3$). Statistical significance in **c-e** was determined by ANOVA, followed by Tukey's HSD test. Data in **c-e** were log-transformed. Significantly differences of means ($P < 0.05$) are represented by different letters. See Source Data for *P* values for **c**, **d** and **e**.

nature research

Corresponding author(s): Julia Bailey-Serres

Last updated by author(s): 04-20-2020

Reporting Summary

Nature Research wishes to improve the reproducibility of the work that we publish. This form provides structure for consistency and transparency in reporting. For further information on Nature Research policies, see Authors & Referees and the Editorial Policy Checklist.

Statistics

For all statistical analyses, confirm that the following items are present in the figure legend, table legend, main text, or Methods section.

n/a	Confirmed	
☐	☒	The exact sample size (*n*) for each experimental group/condition, given as a discrete number and unit of measurement
☐	☒	A statement on whether measurements were taken from distinct samples or whether the same sample was measured repeatedly
☐	☒	The statistical test(s) used AND whether they are one- or two-sided *Only common tests should be described solely by name; describe more complex techniques in the Methods section.*
☒	☐	A description of all covariates tested
☐	☒	A description of any assumptions or corrections, such as tests of normality and adjustment for multiple comparisons
☒	☐	A full description of the statistical parameters including central tendency (e.g. means) or other basic estimates (e.g. regression coefficient) AND variation (e.g. standard deviation) or associated estimates of uncertainty (e.g. confidence intervals)
☐	☒	For null hypothesis testing, the test statistic (e.g. *F*, *t*, *r*) with confidence intervals, effect sizes, degrees of freedom and *P* value noted *Give P values as exact values whenever suitable.*
☒	☐	For Bayesian analysis, information on the choice of priors and Markov chain Monte Carlo settings
☒	☐	For hierarchical and complex designs, identification of the appropriate level for tests and full reporting of outcomes
☒	☐	Estimates of effect sizes (e.g. Cohen's *d*, Pearson's *r*), indicating how they were calculated

Our web collection on statistics for biologists contains articles on many of the points above.

Software and code

Policy information about availability of computer code

Data collection	For growth phenotypes: Canon EOS Rebel T1i camera For microscopy: Keyence BZ-X800, Leica SP5 For qPCR: CFX Connect™ Real-Time PCR Detection System For polysome profile: Brandel Density Gradient Fractionation System For western blots: Biorad Chemidoc MP Imaging system For RNA-seq: Illumina NextSeq500
Data analysis	For phenotype and confocal imaging: LAS X, Fiji software For phylogenetic analysis: MEGA7, Interactive Tree of Life (iTOL) software For polysome profile: Brandel PeakChart software For RNA-seq and RNA decay data: R v3.4, systemPipeR v1.20.0, Bowtie2 v2.2.5, Tophat v2.0.14, edgeR v3.28.1, RNAdecay, ggplot2 v3.3.0, easyGplot2 1.0, ComplexHeatmap 2.2.0 For statistical analysis: R v3.4, agricolae v1.3-2

For manuscripts utilizing custom algorithms or software that are central to the research but not yet described in published literature, software must be made available to editors/reviewers. We strongly encourage code deposition in a community repository (e.g. GitHub). See the Nature Research guidelines for submitting code & software for further information.

Data

Policy information about availability of data

All manuscripts must include a data availability statement. This statement should provide the following information, where applicable:

- Accession codes, unique identifiers, or web links for publicly available datasets
- A list of figures that have associated raw data
- A description of any restrictions on data availability

Uncropped western blots are provided as Source Data Extended Data Figs 2,4.
Raw and processed data associated with Figs 3-5 were deposited into the NCBI GEO database as accession GSE136713

Field-specific reporting

Please select the one below that is the best fit for your research. If you are not sure, read the appropriate sections before making your selection.

☒ Life sciences ☐ Behavioural & social sciences ☐ Ecological, evolutionary & environmental sciences

For a reference copy of the document with all sections, see nature.com/documents/nr-reporting-summary-flat.pdf

Life sciences study design

All studies must disclose on these points even when the disclosure is negative.

Sample size	No sample size-calculation was performed. The sample size was considered based on the feasibility of data collection and data variation within the genotype. We followed standard practice for data replication and statistical analyses. Total RNA- and TRAP-seq samples were prepared from pooled whole plant tissues of over 300 plants per samples. The numbers of plants for each genotype in RNA decay experiment were provided in the Method section.
Data exclusions	No data were excluded from the analyses, with the exception that lowly expressed genes were excluded from the analysis as described in the Methods.
Replication	RNA-seq analysis and RNA half-life determination was performed in three independent biological replicates, with data reproducibility confirmed by PCA and through calculation of p-value and other statistics. Sequencing depth was beyond necessary for detection of low abundance transcripts by RNA-seq. Phenotypic analyses were not repeated as the phenotypes are reproducibly and visually apparent. Protein subcellular localization data were collected from at least three independent experiments with the total number of plants used for each genotype specified in the figure legends. Pathogen infection assay was repeated twice with similar results. Western blots were performed in biological triplicate. Data were reproducible; no datasets were discarded.
Randomization	Samples were grown in the same condition and sorted based on their genotype. The positions of individual plants/plates grown in growth chamber/room were randomized between genotypes.
Blinding	Investigators were not blinded in during data collection; this was not a routine practice during the collection of these data.

Reporting for specific materials, systems and methods

We require information from authors about some types of materials, experimental systems and methods used in many studies. Here, indicate whether each material, system or method listed is relevant to your study. If you are not sure if a list item applies to your research, read the appropriate section before selecting a response.

Materials & experimental systems

n/a	Involved in the study
☐	☒ Antibodies
☒	☐ Eukaryotic cell lines
☒	☐ Palaeontology
☐	☒ Animals and other organisms
☒	☐ Human research participants
☒	☐ Clinical data

Methods

n/a	Involved in the study
☒	☐ ChIP-seq
☒	☐ Flow cytometry
☒	☐ MRI-based neuroimaging

Antibodies

Antibodies used	Monoclonal ANTI-FLAG M2 antibody (Sigma F1804); Polyclonal antibodies recognizing specific peptides of RH6, RH8 or RH12 were a gift from Cécile Bousquet-Antonelli. We cited the paper where the preparation of these was described and dilutions used.
Validation	According to the manufacturer, the ANTI-FLAG M2 mouse affinity purified monoclonal antibody binds to fusion proteins

containing a FLAG peptide sequence, with the binding site:N-Asp-Tyr-Lys-Asp-Asp-Asp-Asp-Lys-C. Our results with mutants confirmed the specificity of the antibodies prepared against the three RHs.

Animals and other organisms

Policy information about studies involving animals; ARRIVE guidelines recommended for reporting animal research

Laboratory animals	Hyaloperonospora arabidopsidis Noco2
Wild animals	The study did not involve wild animals.
Field-collected samples	The study did not include field-collected samples.
Ethics oversight	No ethical approval or guidance was needed for this study on plants and with bacteria.

Note that full information on the approval of the study protocol must also be provided in the manuscript.